





ORIGINAL RESEARCH

# CCL17 Protects Against Viral Myocarditis by Suppressing the Recruitment of Regulatory T Cells

Guoshuai Feng , PhD; Cuige Zhu, PhD; Chieh-Yu Lin , MD, PhD; Andrea Bredemeyer, PhD; Irmgard Förster , PhD; Daniel Kreisel, MD, PhD; Kory J. Lavine , MD, PhD

**BACKGROUND:** Viral myocarditis is characterized by leukocyte infiltration of the heart and cardiomyocyte death. We recently identified C-C chemokine ligand (CCL) 17 as a proinflammatory effector of C-C chemokine receptor 2–positive macrophages and dendritic cells that are recruited to the heart and contribute to adverse left ventricular remodeling following myocardial infarction and pressure overload.

**METHODS AND RESULTS:** Mouse encephalomyocarditis virus was used to investigate the function of CCL17 in a viral myocarditis model. *Ccl17<sup>Gfp</sup>* reporter and knockout mice were used to identify the cell types that express CCL17 and delineate the functional importance of CCL17 in encephalomyocarditis virus clearance and myocardial inflammation. Cardiac CCL17 was expressed in C-C chemokine receptor 2–positive macrophages and dendritic cells following encephalomyocarditis virus infection. Colony-stimulating factor 2 (granulocyte-macrophage colony-stimulating factor) signaling was identified as a key regulator of CCL17 expression. *Ccl17* deletion resulted in impaired encephalomyocarditis virus clearance, increased cardiomyocyte death, and higher mortality during infection early stage, and aggravated hypertrophy and fibrotic responses in infection long-term stage. An increased abundance of regulatory T cells was detected in the myocardium of injured *Ccl17*-deficient mice. Depletion of regulatory T cells in *Ccl17*-deficient mice abrogated the detrimental role of CCL17 deletion by restoring interferon signaling.

**CONCLUSIONS:** Collectively, these findings identify CCL17 as an important mediator of the host immune response during cardiac viral infection early stage and suggest that CCL17 targeted therapies should be avoided in acute viral myocarditis.

**Key Words:** C-C chemokine ligand 17 ■ macrophages ■ monocyte ■ myocardial inflammation ■ regulatory T-cell recruitment ■ virus clearance

**V**iral myocarditis is pathologically defined as myocardial inflammation and cardiomyocyte death induced by viral infection that is clinically associated with ventricular arrhythmias and dysfunction, sudden death, and future heart failure. Myocardial inflammation is characterized by infiltration of leukocytes, including monocytes, macrophages, and lymphocytes, in areas of cardiomyocyte necrosis. Viral myocarditis is heterogeneous in regard to involved myocardial territories (localized or diffuse) and temporal course (acute, subacute, or chronic).<sup>1</sup> The immunologic mechanisms

that contribute to pathogen clearance, inflammatory host responses, and clinical sequelae of viral myocarditis remain incompletely defined.

The host immune response triggered by viral infection is characterized by infiltration of monocytes, macrophages, dendritic cells, and naïve and virus-specific T lymphocytes. Early innate and adaptive immune responses are thought to be beneficial and limit viral propagation.<sup>2</sup> Excessive and persistent inflammatory responses may contribute to collateral myocardial injury, maladaptive cardiac remodeling,

Correspondence to: Kory J. Lavine, MD, PhD, Division of Cardiology, Department of Medicine, Washington University School of Medicine, 660 S Euclid, Campus Box 8086, St. Louis, MO 63110. Email: [klavine@wustl.edu](mailto:klavine@wustl.edu)

Supplemental Material is available at <https://www.ahajournals.org/doi/suppl/10.1161/JAHA.122.028442>

For Sources of Funding and Disclosures, see page 14.

© 2023 The Authors. Published on behalf of the American Heart Association, Inc., by Wiley. This is an open access article under the terms of the [Creative Commons Attribution-NonCommercial-NoDerivs](https://creativecommons.org/licenses/by-nc-nd/4.0/) License, which permits use and distribution in any medium, provided the original work is properly cited, the use is non-commercial and no modifications or adaptations are made.

JAHA is available at: [www.ahajournals.org/journal/jaha](http://www.ahajournals.org/journal/jaha)

## CLINICAL PERSPECTIVE

### What Is New?

- C-C chemokine ligand 17 is an inflammatory mediator expressed in macrophages and dendritic cells recruited to the myocarditis heart.
- Colony-stimulating factor 2 signaling is a key regulator of C-C chemokine ligand 17 expression in C-C chemokine receptor 2-positive macrophages and dendritic cells recruited to the heart during myocarditis.
- *Ccl17* deletion attenuates inflammatory cytokine/chemokine expression, aggravates myocardial fibrosis, and leads to cardiomyocyte death in mouse model of encephalomyocarditis virus infection through increased recruitment of regulatory T cells to the infected heart.

### What Are the Clinical Implications?

- Identification of effector molecules that mediate adverse effects of C-C chemokine receptor 2-positive monocytes, macrophages, and dendritic cells provides new insights into therapeutic strategies to regulate myocardial inflammation.
- Blockade of C-C chemokine ligand 17 should be avoided in the case of acute viral myocarditis as promotion on regulatory T-cell recruitment and results in immunosuppression and delayed viral clearance.

## Nonstandard Abbreviations and Acronyms

<b>CCL</b>	C-C chemokine ligand
<b>CCR</b>	C-C chemokine receptor
<b>EMCV</b>	encephalomyocarditis virus
<b>G1</b>	gate 1
<b>G2</b>	gate 2
<b>G3</b>	gate 3
<b>G4</b>	gate 4
<b>GFP</b>	green fluorescent protein
<b>LY6C</b>	lymphocyte antigen 6 complex, locus C
<b>Treg</b>	regulatory T cell

and resultant heart failure.<sup>3</sup> The appropriateness and efficacy of immunosuppression for viral myocarditis remain controversial.<sup>4</sup> Investigation of experimental animal models and human pathology specimens has revealed that monocytes, macrophages, and dendritic cells contribute to the initial host immune response to infection.<sup>5–8</sup> The adaptive immune response is largely governed by T cells. Intriguingly, deficiency of cluster of differentiation (CD) 8 T cells aggravated myocarditis, whereas loss of CD4 T cells resulted in protection from

coxsackievirus B3-induced myocarditis, suggesting that different T-cell subsets may have distinct functions in virus myocarditis.<sup>9,10</sup>

Chemokines regulate leukocyte trafficking and, thus, represent a promising therapeutic target to favorably manipulate immune responses and avoid the deleterious consequences of excessive myocardial inflammation.<sup>11,12</sup> For example, inhibition of monocyte recruitment to the heart through manipulation of C-C chemokine receptor (CCR) 2 signaling attenuates myocarditis in mouse models.<sup>6–8</sup> C-C chemokine ligand (CCL) 17 has previously been reported to influence CD4 effector and regulatory T-cell (Treg) recruitment by activating the G-protein-coupled receptor CCR4.<sup>13,14</sup> CCL17 signaling is associated with numerous inflammatory diseases, including asthma,<sup>15</sup> dermatitis,<sup>16</sup> colitis,<sup>17</sup> arthritis,<sup>18–20</sup> and atherosclerosis.<sup>21</sup> We previously identified CCL17 as an effector of CCR2<sup>+</sup> macrophages and dendritic cells that was induced following myocardial infarction and pressure overload-induced heart failure. Within these disease contexts, CCL17 amplified tissue inflammation by suppressing the recruitment of Tregs.<sup>17,21,22</sup>

The above studies indicate that inhibition of CCL17 signaling may represent an attractive therapeutic strategy to resolve myocardial inflammation and suppress heart failure progression by augmenting Treg recruitment. Proper implementation of CCL17 inhibition will require an understanding of the cardiac disease entities that are amenable to targeting this signaling pathway. Myocarditis represents an important contributor to cardiac mortality and heart failure, particularly in young patients.<sup>1</sup> The role of CCL17 in viral myocarditis remains to be defined.

In this study, we used a mouse model of experimental viral myocarditis using cardiotropic encephalomyocarditis virus (EMCV). We show that CCL17 is expressed in CCR2<sup>+</sup> macrophages and dendritic cells that infiltrate the heart after EMCV infection. CCL17 expression was regulated by colony-stimulating factor 2 (CSF2/granulocyte-macrophage colony-stimulating factor) signaling. We identified a protective role for CCL17. Deletion of *Ccl17* increased viral load, enhanced myocardial inflammation and cardiomyocyte death during acute infection, and aggravated hypertrophy and fibrosis in the following chronic stage. *Ccl17*-deficient mice displayed increased Treg recruitment, and depletion of Tregs abrogated the deleterious effect of CCL17 deletion by restoring interferon signaling. Collectively, these findings suggest that CCL17-targeted therapies should be avoided in acute viral myocarditis.

## METHODS

The data that support the findings of this study are available from the corresponding author upon

reasonable request. Detailed descriptions of the materials and methods are available in Data S1.

## Animal Studies

Mice were bred and maintained at Washington University School of Medicine, and all experimental procedures were done in accordance with the animal use oversight

committee. Mouse strains used included *Ccl17<sup>Gfp</sup>*,<sup>23</sup> *Foxp3-Dtr*,<sup>24</sup> and *Zbtb46<sup>Gfp</sup>*.<sup>25</sup> All mice were on the C57BL/6J background, and males and females were included in all experiments. Myocarditis was induced by administering  $10^4$  plaque forming units EMCV-D virus via intraperitoneal injection.<sup>26</sup> Information of all mouse primers used in this study is provided in Table S1.

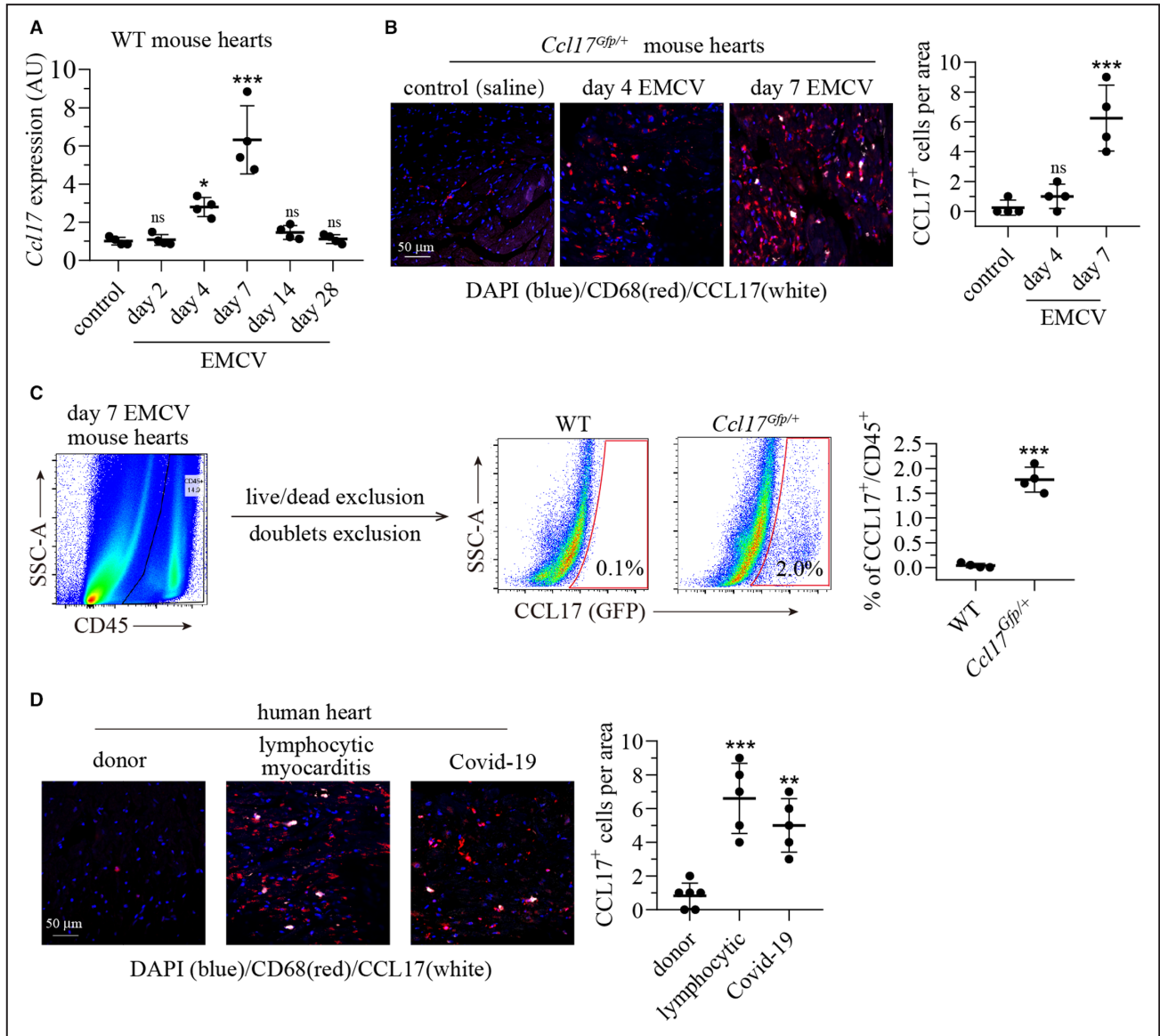


**Figure 1. CCL17 is expressed following EMCV infection.**

**A**, Quantitative reverse transcription–polymerase chain reaction measuring *Ccl17* mRNA expression in hearts of WT mice 2, 4, 7, 14, and 28 days after EMCV ( $n=4$ ) or saline (control;  $n=4$ ) administration. **B**, Immunostaining for CCL17–GFP (white), CD68 (red), and DAPI (blue), showing the spatial distribution of GFP<sup>+</sup> CCL17 expressing cells in hearts of *Ccl17<sup>Gfp/+</sup>* mice 4 and 7 days after EMCV or saline administration. **C**, Flow cytometry revealing GFP<sup>+</sup> (CCL17-expressing) immune cells (gated on CD45<sup>+</sup> cells) in hearts of WT and *Ccl17<sup>Gfp/+</sup>* mice 7 days after EMCV injection. **D**, Immunostaining for CCL17 (white), CD68 (red), and DAPI (blue), showing the spatial distribution of CCL17-expressing cells in healthy donor hearts ( $n=6$ ), lymphocytic myocarditis hearts ( $n=5$ ), and COVID-19 cardiomyopathy hearts ( $n=5$ ). For comparisons between 2 groups that did not present normality (**C**), unpaired *t* test with Welch correction was performed. For multiple comparisons that presented normality, ordinary 1-way ANOVAs, following Tukey tests, for **A** and **D** (equal variance) were performed. For multiple comparisons that did not present normality (**B**), nonparametric Kruskal-Wallis tests were performed. All data are mean $\pm$ SD. AU indicates arbitrary unit; CCL, C-C chemokine ligand; CD, cluster of differentiation; DAPI, 4',6-diamidino-2-phenylindole; EMCV, encephalomyocarditis virus; GFP, green fluorescent protein; ns, nonsignificance; SSC, side scatter; and WT, wild type. \* $P<0.05$ , \*\* $P<0.01$ , and \*\*\* $P<0.001$ .

## Human Studies

Myocardial tissue was obtained following left ventricular assist device implantation or heart transplantation. The study was approved by the Washington University Institutional Review Board (study number 201104172). All subjects provided informed consent before sample collection, and the experiments were performed in accordance with the approved study protocol. Information of all patients with COVID-19 in this study is provided in [Table S2](#).

## Statistical Analysis

Comparisons between groups were calculated by *t* tests or ordinary 1-way ANOVA following Tukey test (equal variance) and Welch ANOVA following Games-Howell test (unequal variance). Sample size, replicates, and statistical tests are documented in the figure legends.

## RESULTS

### EMCV Infection Triggers CCL17 Expression Within the Heart

To examine whether CCL17 expression is induced in the setting of viral myocarditis, we infected mice with EMCV ( $10^4$  pfu, intraperitoneally). Quantitative reverse transcription–polymerase chain reaction (RT-PCR) revealed that *Ccl17* mRNA expression increased over time, peaking at 7 days and returning to baseline 28 days following EMCV infection ([Figure 1A](#)). The time course of *Ccl17* mRNA expression coincided with EMCV viral load and interferon activation, as assessed by viral RNA and 2'-5'-oligoadenylate synthetase 2 (*Oas2*) mRNA expression ([Figure S1A](#)). Immunostaining of *Ccl17<sup>Gfp/+</sup>* reporter mice revealed GFP (green fluorescent protein) expression in CD68<sup>+</sup> cells (monocytes, macrophages, and dendritic cells) within the myocardium of EMCV-infected animals ([Figure 1B](#)).

Flow cytometric analysis indicated that ≈2% of CD45<sup>+</sup> cells expressed GFP in EMCV-injured heart ([Figure 1C](#); [Figure S1B](#)). Immunostaining of human myocardial samples obtained from patients with lymphocytic or COVID-19 myocarditis demonstrated the presence of CCL17<sup>+</sup> CD68<sup>+</sup> cells within the myocardium. No CCL17 expression was observed in donor controls ([Figure 1D](#)). Elevated troponin I was found in plasma of patients infected with COVID-19 who died with acute respiratory distress syndrome ([Table S2](#)). Collectively, these data indicate that CCL17 is expressed in CD68<sup>+</sup> cells in the context of viral myocarditis.

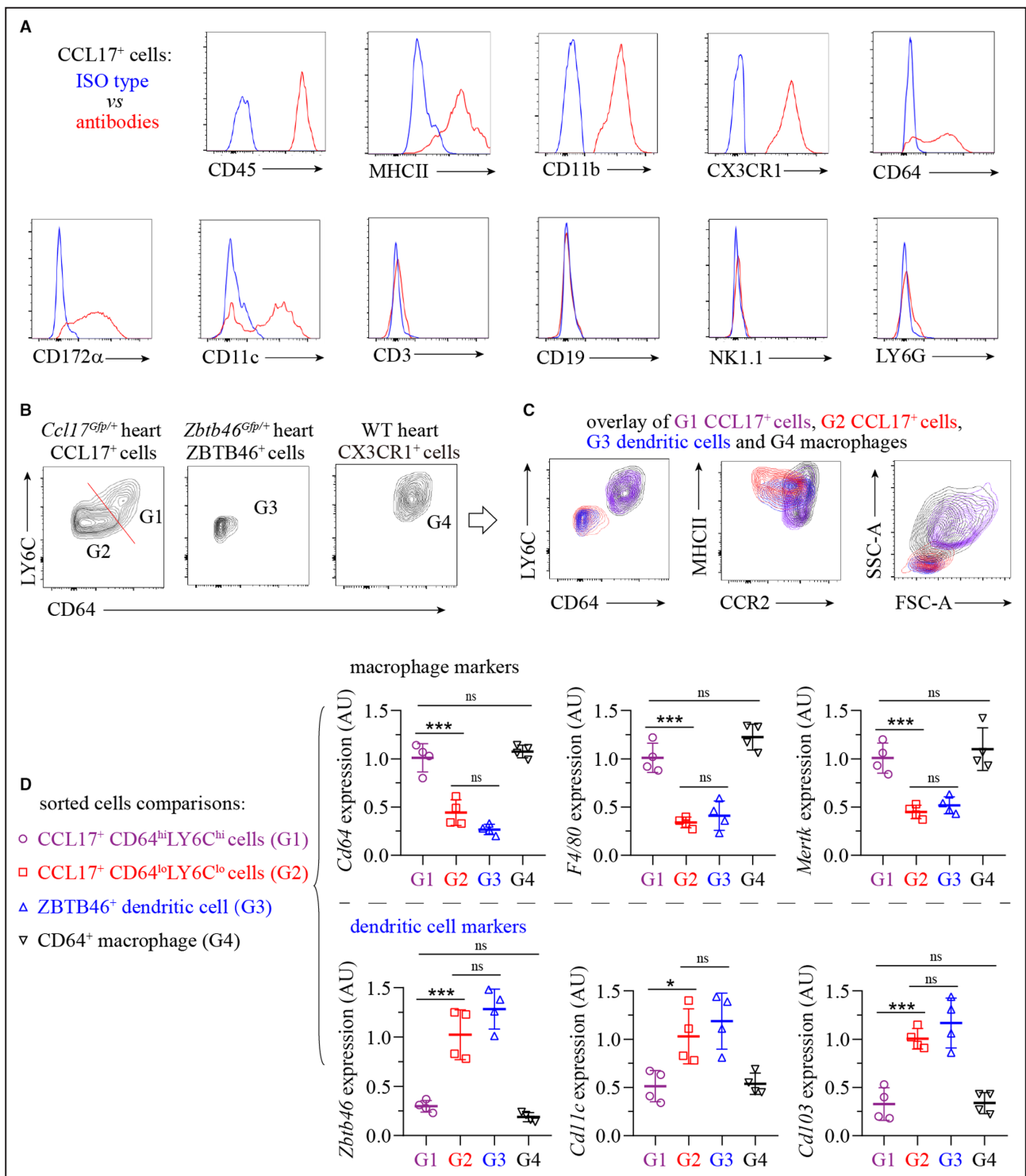
### CCL17 Is Expressed in Macrophages and Dendritic Cells Within the Heart Following EMCV Infection

To define the precise immune cell types that express CCL17, EMCV-infected *Ccl17<sup>Gfp/+</sup>* hearts were analyzed by flow cytometry. We observed GFP expression in immune cells (CD45) that expressed markers of antigen-presenting cells (major histocompatibility complex class II), myeloid cells (CD11b), macrophages (CX3CR1 and CD64), and dendritic cells (CD172 $\alpha$  and CD11c). GFP expression was not detected in T cells (CD3), B cells (CD19), natural killer cells (NK1.1), or neutrophils (lymphocyte antigen 6 complex, locus G6D) ([Figure 2A](#)). These data suggest that macrophages and dendritic cells express CCL17.

Flow cytometry further identified 2 populations of CCL17<sup>+</sup> cells: CD64<sup>hi</sup> lymphocyte antigen 6 complex, locus C (LY6C)<sup>hi</sup> (gate 1 [G1]) and CD64<sup>lo</sup>LY6C<sup>lo</sup> (gate 2 [G2]) cells ([Figure 2B](#), left panel; [Figure S2A](#)). Previous studies have suggested that CCL17 is expressed in macrophages and dendritic cells, depending on the tissue and disease context.<sup>22,23,27</sup> To rigorously distinguish dendritic cells from macrophages, we used *Zbtb46<sup>Gfp/+</sup>* reporter mice, which express GFP specifically in dendritic cells (gate 3 [G3]) and not in macrophages or

### Figure 2. CCL17 is expressed in C-C chemokine receptor 2–positive macrophages and conventional dendritic cells recruited to EMCV-infected hearts.

**A**, GFP expression test of immune cells, including leukocytes (CD45), lymphocytes (CD3, CD19, and NK1.1), myeloid cells (LY6G, CD11b, CX3CR1, CD64, CD172 $\alpha$ , and CD11c), and antigen-presenting cells (MHC-II) in hearts of *Ccl17<sup>Gfp/+</sup>* mice 7 days after EMCV injection. Red, antibodies. Blue, corresponding isotype antibodies. **B**, Flow cytometry demonstrating CCL17<sup>+</sup>CD64<sup>high</sup> and lymphocyte antigen 6 complex locus C1<sup>high</sup> (CCL17<sup>+</sup>CD64<sup>hi</sup>LY6C<sup>hi</sup>; G1), CCL17<sup>+</sup>CD64<sup>low</sup>LY6C<sup>low</sup> (G2) cells, ZBTB46<sup>+</sup>CD64<sup>low</sup>LY6C<sup>low</sup> dendritic cells (G3), and CX3CR1<sup>+</sup>CD64<sup>hi</sup>LY6C<sup>hi</sup> cells (G4) in hearts of *Ccl17<sup>Gfp/+</sup>* mice, *Zbtb46<sup>Gfp/+</sup>*, and WT mice 7 days after EMCV injection. **C**, Flow cytometry overlay plots of CCL17<sup>+</sup> G1 and G2 cells with ZBTB46<sup>+</sup> dendritic cells (G3) and macrophages (G4). **D**, Quantitative reverse transcription–polymerase chain reaction measuring characteristic macrophage markers (*Cd64*, *F4/80*, and *MertK*) and dendritic cell markers (*Zbtb46*, *Cd11c*, and *Cd103*) in fluorescence-activated cell sorting G1, G2, G3, and G4 cells. For all experiments, 4 mice in each group were treated identically, and hearts were harvested on the same day in 1 experiment to make the comparisons parallelly. For multiple comparisons in **(D)**, all data are mean $\pm$ SD and presented normality. Ordinary 1-way ANOVA, following Tukey multiple comparisons tests for *Cd64*, *F4/80*, *MertK*, *Cd11c*, and *Cd103* (equal variance), and Welch ANOVA, followed by Games-Howell tests for *Zbtb46* (unequal variance), were performed. AU indicates arbitrary unit; CCL, C-C chemokine ligand; CD, cluster of differentiation; CX3CR1, cx3c chemokine receptor 1; DAPI, 4',6-diamidino-2-phenylindole; EMCV, encephalomyocarditis virus; F4/80, EGF-like module-containing mucin-like hormone receptor-like 1; G1, gate 1; G2, gate 2; G3, gate 3; G4, gate 4; GFP, green fluorescent protein; LY6G, lymphocyte antigen 6 complex locus G; MertK, proto-oncogene tyrosine-protein kinase MER; MHC-II, major histocompatibility complex class II; NK1.1, natural killer 1.1; ns, nonsignificance; WT, wild-type; and ZBTB46, zinc finger and BTB domain containing 46. \**P*<0.05 and \*\*\**P*<0.001.



monocytes<sup>25</sup> (Figure 2B, middle panel; Figure S2B). CX3CR1<sup>+</sup>CD64<sup>+</sup>LY6C<sup>+</sup> cells were considered to represent macrophages (gate 4 [G4]) (Figure 2B, right panel; Figure S2C). We used these bona fide dendritic cell (G3) and macrophage (G4) cell populations as references. The 2 CCL17<sup>+</sup> populations (G1 and G2) displayed distinct levels of CD64, LY6C, major histocompatibility complex class II, and CCR2 expression and disparate physical

properties (forward and side scatter) (Figure 2C). The G2 population displayed levels of CD64, LY6C, major histocompatibility complex class II, and CCR2 expression and physical properties that were comparable to dendritic cells (G3), whereas the G1 population displayed levels of CD64, LY6C, major histocompatibility complex class II, and CCR2 expression and disparate physical

To further validate that the G1 and G2 populations represent macrophages and dendritic cells, respectively, we isolated RNA from G1, G2, G3, and G4 cells. Quantitative RT-PCR demonstrated that G1 cells expressed high levels of macrophage markers (*Cd64*, *F4/80*, and *MertK*) and low levels of dendritic cell markers (*Zbtb46*, *Cd11c*, and *Cd103*). In contrast, G2 cells expressed low levels of macrophage markers (*Cd64*, *F4/80*, and *MertK*) and high levels of dendritic cell markers (*Zbtb46*, *Cd11c*, and *Cd103*). For each of these markers, we observed no significant difference between either G1 and G4 cells or G2 and G3 cells (Figure 2D). Collectively, these data suggest that CCL17<sup>+</sup>CD64<sup>hi</sup>LY6C<sup>hi</sup> (G1) cells are macrophages and CCL17<sup>+</sup>CD64<sup>lo</sup>LY6C<sup>lo</sup> (G2) cells are dendritic cells. These findings are consistent with the identity of CCL17<sup>+</sup> cells in models of sterile cardiac injury (myocardial infarction and hypertensive heart disease).<sup>22</sup>

### CSF2 Signaling Regulates CCL17 Expression in CCR2<sup>+</sup> Cardiac Macrophages and Dendritic Cells

We previously found that *Ccl17* is expressed in CCR2<sup>+</sup> macrophages and dendritic cells in human ischemic cardiomyopathy and mouse models of cardiomyocyte depletion, myocardial infarction, and hypertensive heart.<sup>22,28</sup> To determine whether *Ccl17* is similarly expressed in CCR2<sup>+</sup> macrophages and dendritic cells in our myocarditis model, we performed flow cytometric analysis of single cells digested from hearts of EMCV-infected *Ccl17*<sup>Gfp/+</sup> reporter mice. Among CX3CR1<sup>+</sup> macrophages and dendritic cells, most CCL17<sup>+</sup> cells expressed CCR2 (Figure 3A; Figure S3A). CCL17<sup>+</sup>CCR2<sup>+</sup> macrophages and dendritic cells represent a relatively small population, comprising ≈6% of all CX3CR1<sup>+</sup> cells.

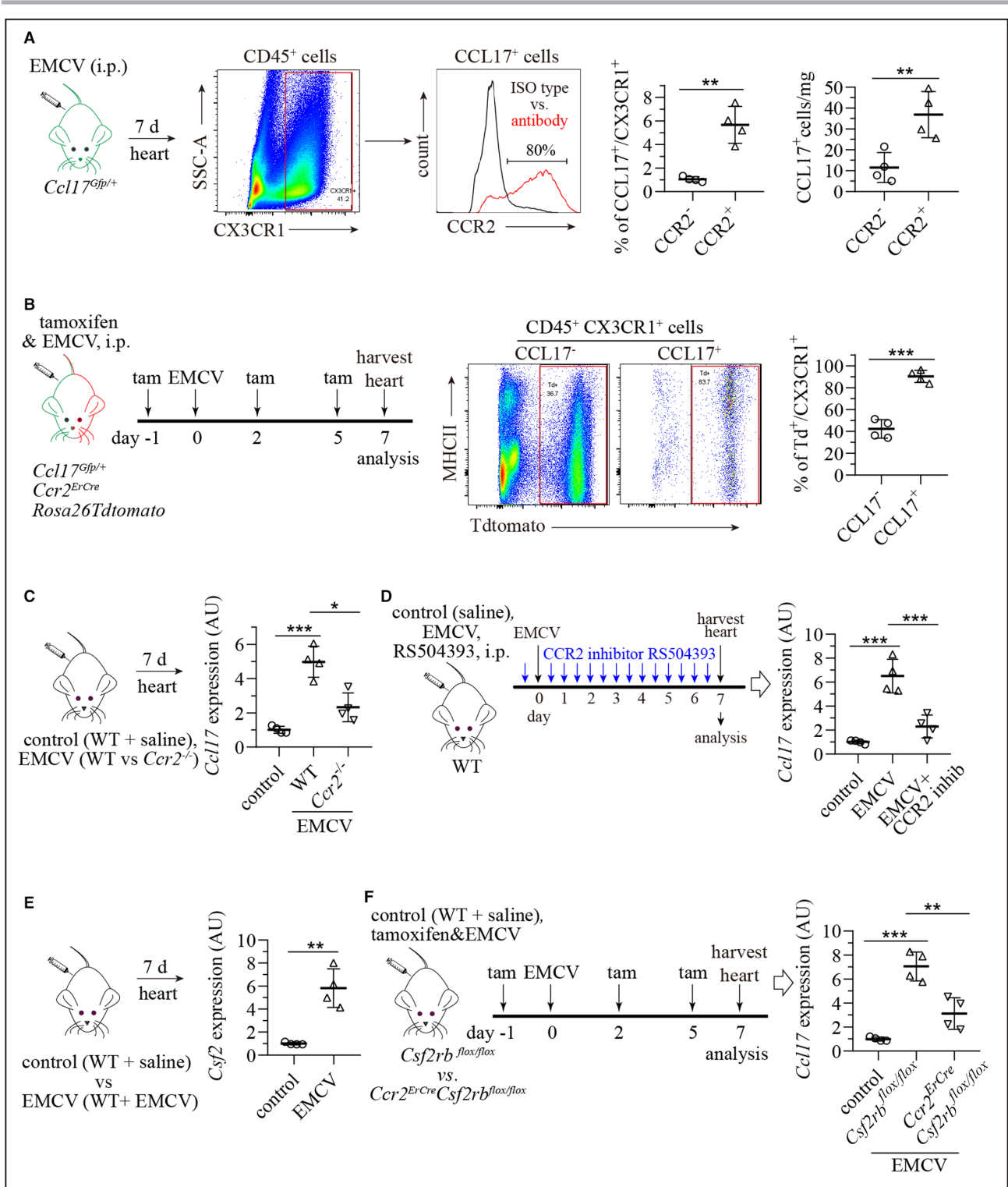
To further substantiate that CCL17<sup>+</sup> macrophages and dendritic cells were derived from infiltrating CCR2<sup>+</sup> monocytes, we generated *Ccl17*<sup>Gfp/+</sup>*Ccr2*<sup>ErCre</sup>*Rosa26*<sup>Tdtomato</sup>

mice, which can be used to track the fate of infiltrating monocytes. Administration of tamoxifen (60 mg/kg, intraperitoneally) every 3 days results in continuous labeling of circulating monocytes without labeling tissue-resident macrophages in heart (Figure S3B). Flow cytometric analysis showed that most CCL17<sup>+</sup> macrophages and dendritic cells were labeled with Tdtomato, indicating that CCL17<sup>+</sup> macrophages and dendritic cells are derived from circulating monocytes and infiltrate the heart following EMCV infection (Figure 3B). Examination of CCL17 expression in circulating leukocytes revealed that CCL17 expression was initiated in the CCR2<sup>+</sup> monocyte blood pool. We did not detect CCL17 expression within the bone marrow compartment (Figure S3C). To provide functional data supporting the conclusion that CCL17<sup>+</sup> macrophages and dendritic cells are derived from infiltrating monocytes, we inhibited CCR2 signaling following EMCV infection. Both deletion of *Ccr2* and pharmacological inhibition of CCR2 signaling (RS504393) resulted in a decrease of *Ccl17* mRNA expression in mouse hearts 7 days after EMCV infection (Figure 3C and 3D).

We previously demonstrated that CSF2 (granulocyte-macrophage colony-stimulating factor) signaling regulated CCL17 in the context of sterile myocardial injury.<sup>22</sup> We next examined whether CSF2 signaling similarly regulated CCL17 expression during myocarditis. We observed increased myocardial *Csf2* mRNA expression 7 days after EMCV infection (Figure 3E). To investigate the functional requirement for CSF2 signaling, we infected *Csf2rb*<sup>flox/flox</sup> and *Ccr2*<sup>ErCre</sup>*Csf2rb*<sup>flox/flox</sup> mice with EMCV and measured CCL17 expression. Mice received tamoxifen every 3 days to delete *Csf2rb* in monocytes and their progeny. Quantitative RT-PCR revealed reduced *Ccl17* mRNA expression in infected *Ccr2*<sup>ErCre</sup>*Csf2rb*<sup>flox/flox</sup> hearts compared with *Csf2rb*<sup>flox/flox</sup> (Figure 3F). Collectively, these data indicate that CSF2 signaling regulates CCL17 expression in CCR2<sup>+</sup> macrophages and dendritic cells during myocarditis.

### Figure 3. CSF2 signaling in monocytes regulates the specification of CCL17<sup>+</sup> macrophage and dendritic cells.

**A**, Flow cytometry identifying CCL17 expression in CCR2<sup>+</sup> and CCR2<sup>-</sup> leukocytes. *Ccl17*<sup>Gfp/+</sup> mice hearts were harvested and digested for analysis 7 days after EMCV injection. CCL17<sup>+</sup> cells were gated from CD45<sup>+</sup> cells and checked with CCR2 antibody (red) and corresponding isotype antibody (black). The 2 dot plots on the right showed CCL17<sup>+</sup> cell proportion and count of CCR2<sup>+</sup> and CCR2<sup>-</sup> myeloid cells (CX3CR1<sup>+</sup>). **B**, Flow cytometry identifying CCL17 expression in CCR2<sup>+</sup> and CCR2<sup>-</sup> leukocytes. *Ccl17*<sup>Gfp/+</sup> mice were treated with tam and EMCV, and hearts were harvested for analysis. **C**, Quantitative RT-PCR measuring *Ccl17* mRNA expression in hearts of *Ccr2*<sup>+/+</sup>, *Ccr2*<sup>-/-</sup>, and normal saline-treated WT mice (as control). **D**, Quantitative RT-PCR measuring *Ccl17* mRNA expression in hearts of WT mice. Mice were treated with EMCV, CCR2 inhib RS504393, or saline (control). **E**, Quantitative RT-PCR measuring *Csf2* mRNA levels in hearts of WT mice treated with EMCV or saline (control). **F**, Quantitative RT-PCR measuring *Ccl17* mRNA levels in hearts of *Csf2rb*<sup>flox/flox</sup> and *Ccr2*<sup>ErCre</sup>*Csf2rb*<sup>flox/flox</sup> mice treated with EMCV and tamoxifen or WT treated with saline (control). N=4 per experimental group, and all data are mean±SD. For 2 groups, data presented normality, and unpaired *t* tests with (A) or without (B) Welch correction were performed. For 2 groups, data did not present normality (E), and Mann-Whitney tests were performed. For multiple comparisons that passed Shapiro-Wilk normality tests, ordinary 1-way ANOVA, following Tukey, test for C (equal variance) and Welch ANOVA, following Games-Howell tests, for D and F (unequal variance) were performed. AU indicates arbitrary unit; CCL, C-C chemokine ligand; *Ccl17*<sup>Gfp/+</sup>, *Ccl17*<sup>green fluorescent protein/+</sup>; CCR2, C-C chemokine receptor 2; *Ccr2*<sup>+/+</sup>, EMCV-treated WT mice; *Ccr2*<sup>-/-</sup>, *Ccr2* deficiency mice; CD, cluster of differentiation; CSF2, colony-stimulating factor 2; *Csf2rb*, CSF2 receptor subunit β; EMCV, encephalomyocarditis virus; ErCre, estrogen receptor T2 and Cre recombinase; inhib, inhibitor; RT-PCR, reverse transcription-polymerase chain reaction; SSC, side scatter; tam, tamoxifen; and WT, wild-type. \**P*<0.05, \*\**P*<0.01, and \*\*\**P*<0.001.



### Ccl17 Deletion Increases Mortality and Aggravates Cardiac Remodeling Following EMCV Infection

To delineate the functional requirement for CCL17 during myocarditis, we infected wild-type ( $Ccl17^{+/+}$ ) control mice and  $Ccl17$ -deficient ( $Ccl17^{Gfp/Gfp}$ ),

abbreviated as  $Ccl17^{G/G}$ ) mice with  $10^4$  pfu EMCV. We observed significantly increased mortality in  $Ccl17^{G/G}$  mice, which died within 8 days compared with wild-type mice (Figure 4A). Terminal deoxynucleotidyl transferase dUTP nick end labeling staining revealed increased cardiomyocyte death in  $Ccl17^{G/G}$  compared with wild-type hearts after infection (Figure 4B).

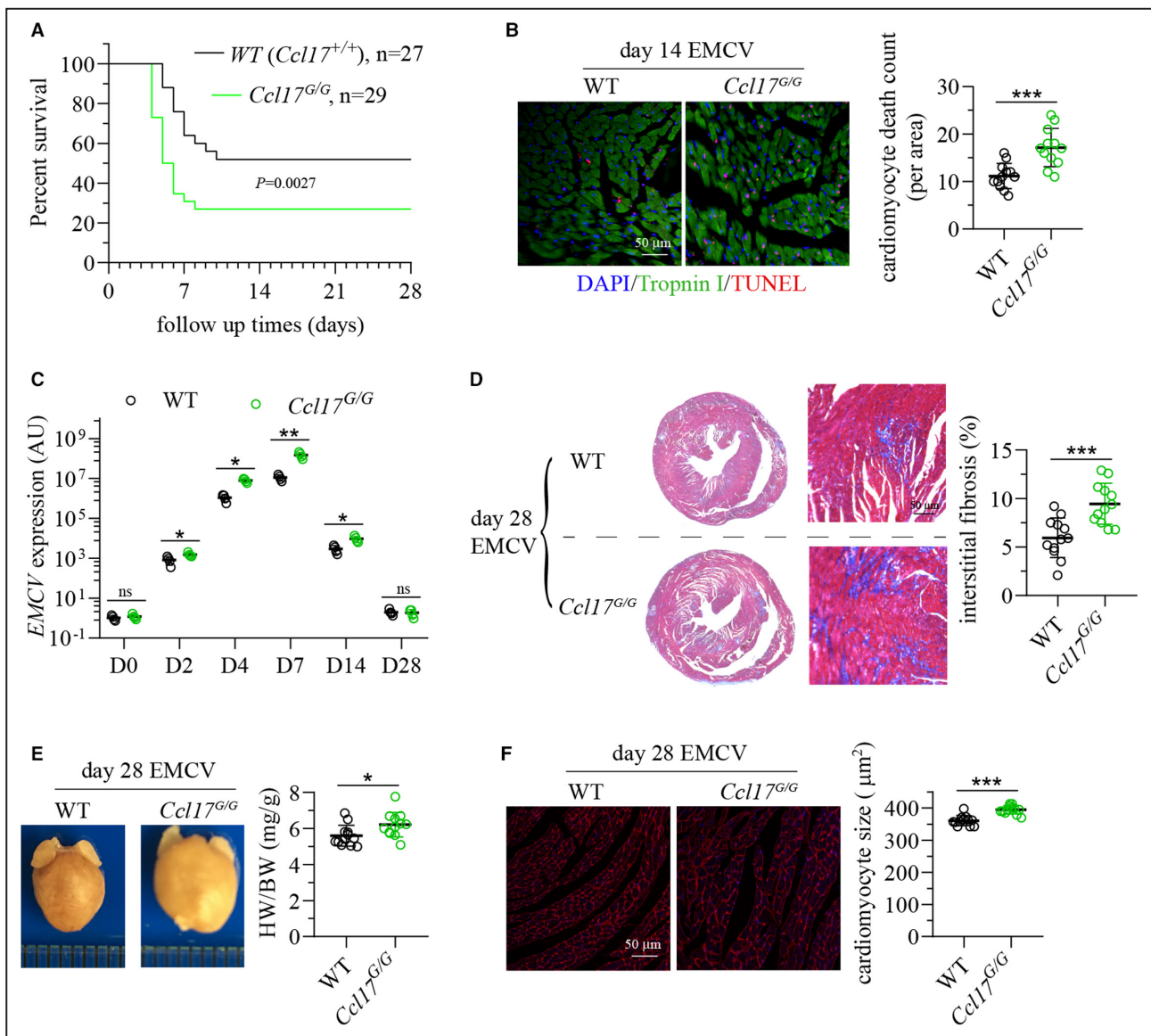


**Figure 4. Ccl17 deletion increases mortality, cardiomyocyte death, and adverse left ventricular remodeling.**

**A**, Post-EMCV survival rate in WT *Ccl17*<sup>+/+</sup> mice and *Ccl17*<sup>G/G</sup> mice. **B**, Representative staining images and quantification for cardiomyocytes (green), DNA-damaged cells (red), and DAPI (blue) showing cardiomyocyte death in WT (n=12) and *Ccl17*<sup>G/G</sup> mice (n=12) 14 days after EMCV injection. **C**, Quantitative reverse transcription-polymerase chain reaction measuring EMCV mRNA levels in hearts of WT mice and *Ccl17*<sup>G/G</sup> mice. **D**, Representative trichrome staining images and quantification of interstitial fibrosis in hearts of WT mice and *Ccl17*<sup>G/G</sup> mice 28 days after EMCV treatment. **E**, Measurement of HW/BW ratio in WT mice and *Ccl17*<sup>G/G</sup> mice 28 days after EMCV injection. **F**, Representative wheat germ agglutinin-stained images showing cardiomyocytes in cross-section (red; left panel) and quantification of cardiomyocyte cross-sectional area (right panel) in hearts of WT mice and *Ccl17*<sup>G/G</sup> mice 28 days after EMCV treatment. All data are mean±SD and presented normally. For survival rate comparison in **A**, log-rank (Mantel-Cox) test was performed. For 2 group comparisons with equal variance (**B** through **F**), unpaired *t* tests were performed. AU indicates arbitrary unit; *Ccl17*<sup>+/+</sup>, C-C chemokine ligand 17<sup>+/+</sup>; *Ccl17*<sup>G/G</sup>, *Ccl17*<sup>green fluorescent protein/green fluorescent protein</sup>; DAPI, 4',6-diamidino-2-phenylindole; and HW/BW, heart weight/body weight. \**P*<0.05, \*\**P*<0.01, and \*\*\**P*<0.001.

Quantitative RT-PCR showed higher EMCV RNA in *Ccl17*<sup>G/G</sup> hearts compared with wild-type hearts at multiple time points after infection, indicating that CCL17 may suppress viral replication and/or promote viral clearance (Figure 4C). Trichrome staining revealed elevated myocardial fibrosis in surviving *Ccl17*<sup>G/G</sup> mice compared with wild-type mice 28 days after EMCV

injection (Figure 4D). Quantification of heart/body weight ratio demonstrated increased size of *Ccl17*<sup>G/G</sup> hearts compared with wild-type hearts 28 days after EMCV infection (Figure 4E). Wheat germ agglutinin staining further showed that *Ccl17*<sup>G/G</sup> hearts displayed increased cardiomyocyte cross-sectional area compared with wild-type hearts 28 days following EMCV



infection (Figure 4F). Consistent with these findings, we observed increased *Nppa*, *Nppb*, *Myh7*, *Col1a1*, and *Col3a1* mRNA expression in EMCV-infected *Ccl17<sup>G/G</sup>* hearts compared with infected wild-type hearts (Figure S4A and S4B). Taken together, these data indicate that *Ccl17* deletion increases mortality and viral RNA load, and accelerates cardiac remodeling, in the context of viral myocarditis.

### **Ccl17 Deletion Results in Increased Recruitment of Tregs to EMCV-Infected Hearts**

To decipher whether *Ccl17* deletion impacts the recruitment of different immune cell subsets to the heart during myocarditis, we performed flow cytometry and immunostaining 7 days after EMCV infection. Flow cytometry did not reveal any differences in the abundance of innate immune cells, including neutrophils, monocytes, and macrophages, between infected wild-type and *Ccl17<sup>G/G</sup>* hearts (Figure S5A and S4B). We next examined T-cell subsets by flow cytometry (Figure 5A; Figure S5C). We did not detect differences in the abundance of total T cells (CD3<sup>+</sup>), helper T cells (CD3<sup>+</sup>CD4<sup>+</sup>), cytotoxic T cells (CD3<sup>+</sup>CD8<sup>+</sup>), type 1 helper T cells (CD3<sup>+</sup>CD4<sup>+</sup>CXCR3<sup>+</sup>), type 2 helper T cells (CD3<sup>+</sup>CD4<sup>+</sup>CCR4<sup>+</sup>), or type 17 helper T cells (CD3<sup>+</sup>CD4<sup>+</sup>CCR6<sup>+</sup>) between control and *Ccl17<sup>G/G</sup>* mice 7 days after EMCV injection (Figure 5A and 5B; Figure S5D). We also did not observe differences in the proportion of CD4 or CD8 T cells displaying an effector memory (CD44<sup>+</sup>CD62L<sup>-</sup>) or central memory (CD44<sup>+</sup>CD62L<sup>+</sup>) phenotype between wild-type and *Ccl17<sup>G/G</sup>* mice 7 days after EMCV injection (Figure S5E). In contrast, we observed a robust increase in the number of CD25<sup>+</sup> forkhead box P3–positive Tregs in infected *Ccl17<sup>G/G</sup>* hearts compared with wild-type hearts (Figure 5B and 5C). These data are consistent with reports indicating that *Ccl17* selectively binds to C-C chemokine receptor 4 (CCR4) expressed on Tregs and functions to regulate their trafficking.<sup>22,29,30</sup>

### **Ccl17 Deficiency Aggravates Myocarditis Through a Treg-Dependent Mechanism**

To determine whether enhanced Treg recruitment is responsible for the detrimental effect of *Ccl17* deficiency on myocarditis, we generated *Ccl17<sup>G/G</sup> Foxp3-Dtr* mice to facilitate Treg depletion studies (Figure 6A). *Ccl17<sup>G/G</sup> Foxp3-Dtr* mice were treated with either normal saline (control) or diphtheria toxin (100 ng/mouse; intraperitoneally) every 2 days. We observed robust depletion of forkhead box P3–positive Tregs in hearts of EMCV-infected *Ccl17<sup>G/G</sup> Foxp3-Dtr* mice treated with diphtheria toxin (Figure S6A). Treg depletion was

sufficient to improve the survival rate of *Ccl17<sup>G/G</sup>* mice (53% versus 38%;  $P=0.018$ ; Figure 6B). The survival of *Ccl17<sup>G/G</sup>* mice lacking Tregs was similar to that of EMCV-infected wild-type mice (Figure S6B). Terminal deoxynucleotidyl transferase dUTP nick end labeling staining revealed reduced cardiomyocyte death in *Ccl17<sup>G/G</sup>* mice lacking Tregs 14 days after EMCV infection (Figure 6C; Figure S6C). Quantitative RT-PCR further showed that *Ccl17<sup>G/G</sup>* mice lacking Tregs had decreased EMCV viral RNA at several time points after infection (Figure 6D). We also observed reduced myocardial fibrosis, heart weight/body weight ratio, cardiomyocyte hypertrophy, and expression of genes associated with cardiac hypertrophy and fibrosis in surviving *Ccl17<sup>G/G</sup>* mice that lacked Tregs 28 days after infection (Figure 6E through 6G; Figure S6D through S6G). Collectively, these data causally link enhanced Treg recruitment to the detrimental effects of *Ccl17* deletion during myocarditis.

### **Tregs Attenuate Interferon Signaling in Ccl17-Deficient Mice**

To explore mechanisms by which enhanced Treg recruitment worsens myocarditis outcomes in *Ccl17*-deficient mice, we first examined whether the abundance of effector immune cells was influenced by Treg depletion. Flow cytometric analysis did not show any significant differences in macrophage and effector T-cell abundance between EMCV-infected wild-type, *Ccl17<sup>G/G</sup> Foxp3-Dtr*+normal saline, and *Ccl17<sup>G/G</sup> Foxp3-Dtr*+diphtheria toxin hearts (Figure S7A and S7B). However, markers of interferon signaling were robustly impacted by both *Ccl17* deletion and Treg depletion. We observed marked upregulation of *Ifn-γ*, *Oas2*, *Mx2*, *Cxcl9*, and *Cxcl10* mRNA expression in EMCV-infected hearts compared with uninfected control hearts. Deletion of *Ccl17* resulted in dramatic reductions in *Ifn-γ*, *Oas2*, *Mx2*, *Cxcl9*, and *Cxcl10* mRNA expression following EMCV infection. Depletion of Tregs from *Ccl17*-deficient hearts restored the expression of *Ifn-γ*, *Oas2*, *Mx2*, *Cxcl9*, and *Cxcl10* (Figure 7A). Furthermore, we observed that the expression of other cytokines and chemokines important in myocarditis, including *Ifn-α*, *Ifn-β*, *Tnfa*, *Ilβ*, *Ccl3*, *Ccl4*, and *Ccl9*,<sup>31</sup> were reduced in infected *Ccl17<sup>G/G</sup>* hearts compared with infected wild-type hearts. The expression of these mediators was also restored following Treg depletion (Figure S7C).

Among the above mediators, interferon- $\gamma$  has an established role in reducing myocarditis severity. Previous studies have suggested that interferon- $\gamma$  may be produced by either macrophages or T cells in this disease context.<sup>32,33</sup> To delineate whether *Ccl17* deficiency and Treg depletion reduced the expression of interferon- $\gamma$  in cardiac macrophages

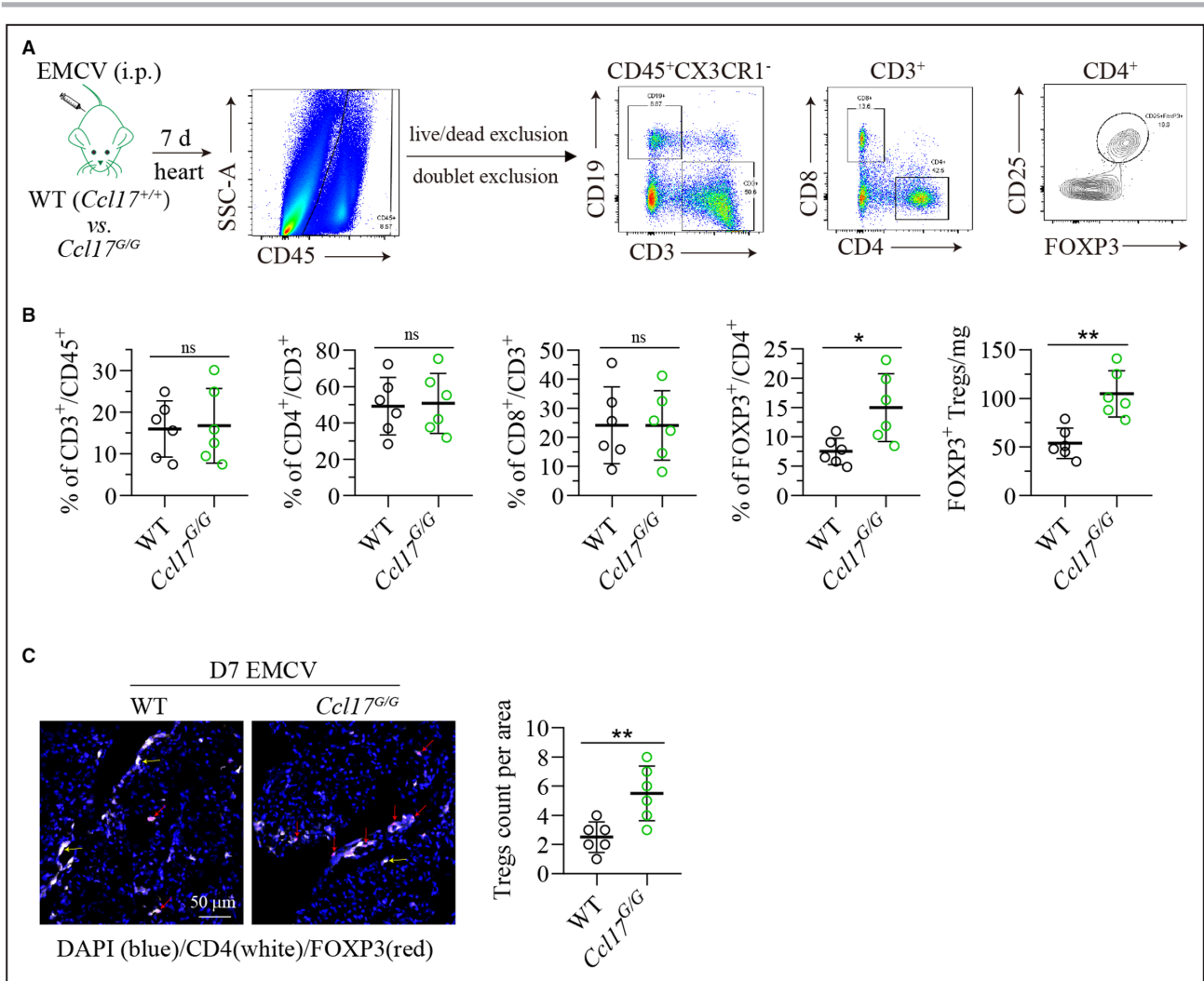


**Figure 5. Ccl17 deficiency increases cardiac Treg abundance following EMCV infection.**

**A**, Flow cytometry gating scheme used to identify CD4<sup>+</sup>FOXP3<sup>+</sup> Tregs. Hearts of WT *Ccl17*<sup>+/+</sup> mice and *Ccl17*<sup>G/G</sup> mice were harvested for analysis 7 days after EMCV infection. **B**, Flow cytometric analysis of the proportion of CD3<sup>+</sup> T cells among CD45<sup>+</sup> leukocytes, CD4<sup>+</sup> helper T cells among CD3<sup>+</sup> T cells, CD8<sup>+</sup> cytotoxic cells among CD3<sup>+</sup> T cells, FOXP3<sup>+</sup> Tregs among CD4<sup>+</sup> helper T cells, and FOXP3<sup>+</sup> Treg count per milligram heart tissue in WT and *Ccl17*<sup>G/G</sup> hearts 7 days after EMCV infection. **C**, Immunostaining for CD4 (white), FOXP3 (red), and DAPI (blue) showing the spatial distribution of Tregs in hearts of WT and *Ccl17*<sup>G/G</sup> mice 7 days after EMCV administration. Yellow arrows, CD4<sup>+</sup> helper T cells. Red arrows, FOXP3<sup>+</sup> Tregs. N=6 per experimental group, and all data are mean±SD. All data presented normality tests and showed equal variance. Unpaired *t* tests were performed in all data. *Ccl17*<sup>+/+</sup> indicates C-C chemokine ligand 17<sup>+/+</sup>; *Ccl17*<sup>G/G</sup>, *Ccl17*<sup>green fluorescent protein/green fluorescent protein</sup>; CD4<sup>+</sup>FOXP3<sup>+</sup>, cluster of differentiation 4 and forkhead box P3 double-positive; DAPI, 4',6-diamidino-2-phenylindole; EMCV, encephalomyocarditis virus; Ns, nonsignificance; SSC, side scatter; Treg, regulatory T-cell; and WT, wild-type. \**P*<0.05 and \*\**P*<0.01.

and T cells, we performed flow cytometry of single cells digested from EMCV-infected wild-type, *Ccl17*<sup>G/G</sup>*Foxp3-Dtr*+normal saline, and *Ccl17*<sup>G/G</sup>*Foxp3-Dtr*+diphtheria toxin hearts. Compared with wild-type conditions, interferon- $\gamma$  expression was significantly reduced in both cardiac macrophages and T cells isolated from infected *Ccl17*<sup>G/G</sup> hearts. Depletion of Tregs from *Ccl17*-deficient hearts restored interferon- $\gamma$  expression to levels that were comparable to infected wild-type hearts (Figure 7B through 7E). Taken together, these findings suggest that enhanced recruitment of Tregs may

potentiate myocarditis by suppressing antiviral immune responses.

## DISCUSSION

We previously identified CCL17 as a proinflammatory mediator of CCR2<sup>+</sup> macrophages and dendritic cells recruited to the heart in mouse models of cardiomyocyte ablation, myocardial infarction, and hypertensive heart disease. In these contexts, *Ccl17* deficiency conferred protection through enhanced Treg recruitment and subsequent attenuation of myocardial

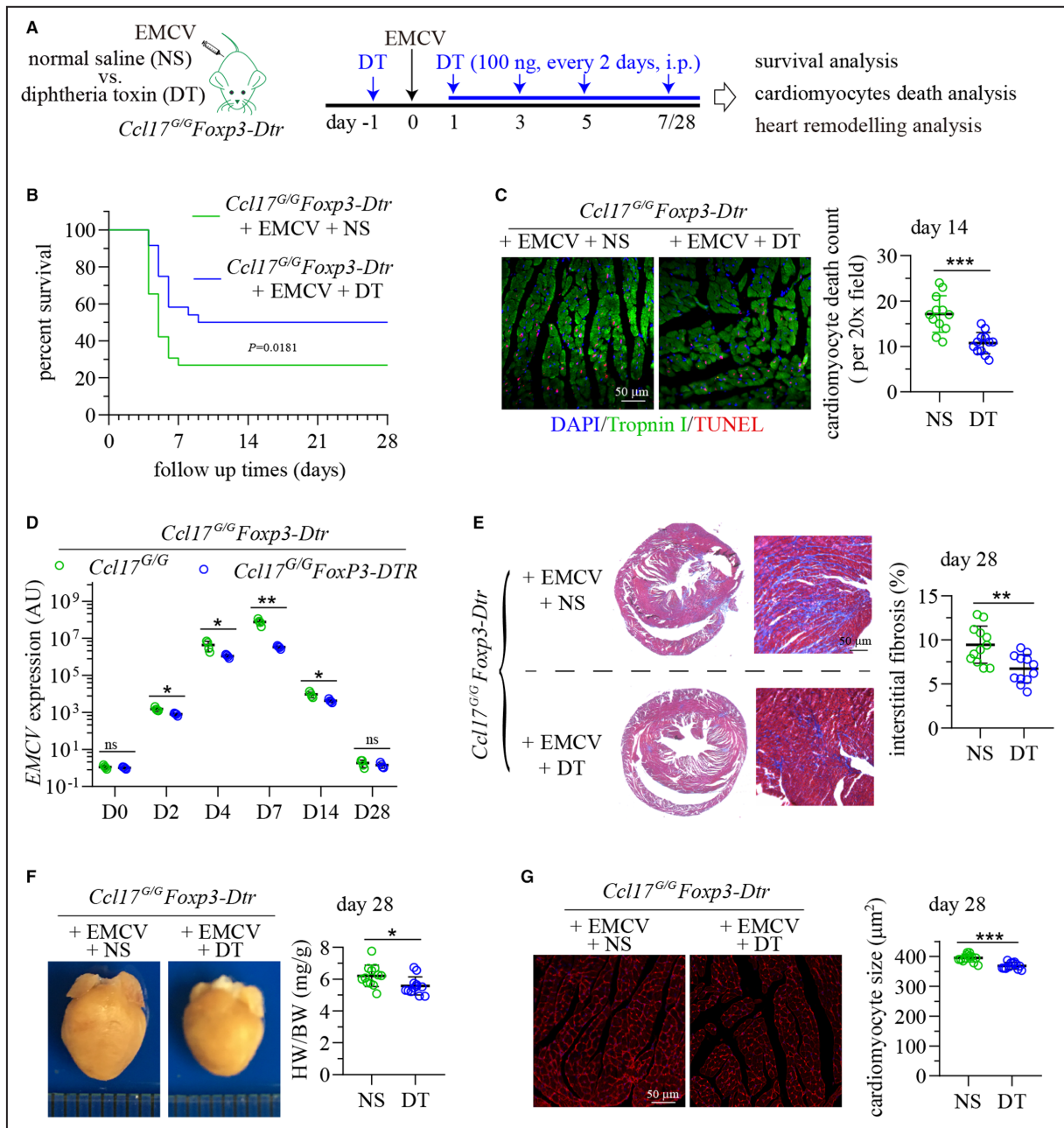
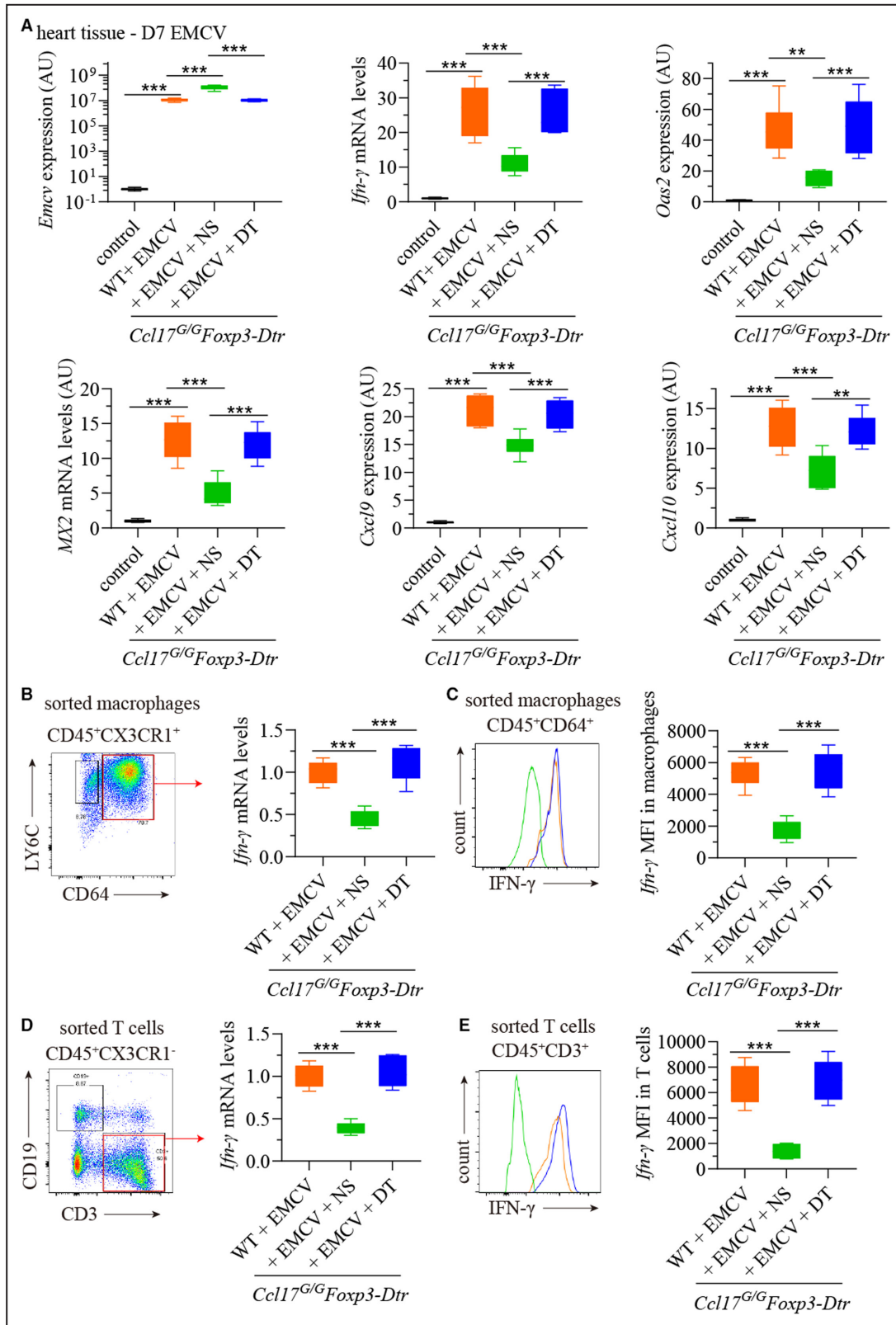


**Figure 6. Tregs mediate the deleterious effects of CCL17 deletion.**

**A**, *Ccl17<sup>G/G</sup>* mice were crossed with *Foxp3-Dtr* mice to generate *Ccl17<sup>G/G</sup>Foxp3-Dtr* mice in which Tregs are deleted after DT administration. *Ccl17<sup>G/G</sup>Foxp3-Dtr* mice were treated with EMCV and DT (or NS) every 2 days. **B**, Post-EMCV survival rate in *Ccl17<sup>G/G</sup>Foxp3-Dtr* mice treated with EMCV, NS, or DT. **C**, Representative staining images and quantification for cardiomyocytes (green), DNA-damaged cells (red), and DAPI (blue) showing cardiomyocyte death in DT (n=12) and NS (n=12) treated *Ccl17<sup>G/G</sup>Foxp3-Dtr* mice 14 days after EMCV injection. **D**, Quantitative reverse transcription–polymerase chain reaction measuring EMCV mRNA levels in hearts of *Ccl17<sup>G/G</sup>Foxp3-Dtr* mice treated with EMCV, NS, or DT. **E**, Representative trichrome staining images and quantification of interstitial fibrosis in hearts of *Ccl17<sup>G/G</sup>Foxp3-Dtr* mice 28 days after EMCV, DT, or NS treatments. **F**, Measurement of HW/BW ratio in *Ccl17<sup>G/G</sup>Foxp3-Dtr* mice 28 days after EMCV, DT, or NS treatments. **G**, Representative wheat germ agglutinin–stained images showing cardiomyocytes in cross-section (red; left panel) and quantification of cardiomyocyte cross-sectional area (right panel) in hearts of *Ccl17<sup>G/G</sup>Foxp3-Dtr* mice 28 days after EMCV, DT, or NS treatments. All data are mean±SD. All data presented normality and showed equal variance. For survival rate comparison in **A**, log-rank (Mantel-Cox) test was performed. For comparisons between 2 groups (**B** through **F**), unpaired *t* tests were performed. CCL indicates C-C chemokine ligand; *Ccl17<sup>G/G</sup>*, *Ccl17<sup>green fluorescent protein/green fluorescent protein</sup>*; DAPI, 4',6-diamidino-2-phenylindole; DT, diphtheria toxin; EMCV, encephalomyocarditis virus; *Foxp3-Dtr*, forkhead box P3–diphtheria toxin receptor; HW/BW, heart weight/body weight; NS, normal saline; Treg, regulatory T-cell; and TUNEL, terminal deoxynucleotidyl transferase dUTP nick end labeling. \**P*<0.05, \*\**P*<0.01, and \*\*\**P*<0.001.



inflammation.<sup>22</sup> These findings highlighted the therapeutic potential of CCL17 inhibition. In this article, we addressed the role of CCL17 in viral myocarditis, an important clinical entity that leads to heart failure in some

individuals. Using EMCV as a model viral pathogen, we found that CCL17 is produced by monocyte-derived macrophages and dendritic cells that infiltrate the myocardium early after viral infection and that CCL17

**Figure 7. CCL17 deletion suppresses IFN signaling through a regulatory T-cell–dependent mechanism.**

**A**, Quantitative RT-PCR measuring *Emcv*, *Ifn- $\gamma$* , *Oas2*, *MX2*, *Cxcl9*, and *Cxcl10* mRNA levels in hearts of NS-treated WT mice (control), EMCV-treated WT mice (WT+EMCV), *Ccl17<sup>G/G</sup>Foxp3-Dtr*+EMCV+NS, and *Ccl17<sup>G/G</sup>Foxp3-Dtr*+EMCV+DT. **B**, Quantitative RT-PCR measuring *Ifn- $\gamma$*  mRNA expression in sorted macrophages from hearts of WT+EMCV mice, *Ccl17<sup>G/G</sup>Foxp3-Dtr*+EMCV+NS mice, and *Ccl17<sup>G/G</sup>Foxp3-Dtr*+EMCV+DT mice. **C**, Representative flow cytometric plot and quantification of intracellular *Ifn- $\gamma$*  expression in sorted CD45<sup>+</sup>CD64<sup>+</sup> macrophages from hearts of WT+EMCV mice, *Ccl17<sup>G/G</sup>Foxp3-Dtr*+EMCV+NS mice, and *Ccl17<sup>G/G</sup>Foxp3-Dtr*+EMCV+DT mice. **D**, Quantitative RT-PCR measuring *Ifn- $\gamma$*  mRNA expression in sorted T cells from hearts of WT+EMCV mice, *Ccl17<sup>G/G</sup>Foxp3-Dtr*+EMCV+NS mice, and *Ccl17<sup>G/G</sup>Foxp3-Dtr*+EMCV+DT mice. **E**, Representative flow cytometric plot and quantification of intracellular *Ifn- $\gamma$*  expression in sorted T cells from hearts of WT+EMCV mice, *Ccl17<sup>G/G</sup>Foxp3-Dtr*+EMCV+NS mice, and *Ccl17<sup>G/G</sup>Foxp3-Dtr*+EMCV+DT mice. N=6 per group, and all data are mean $\pm$ SD. All data presented normality. Welch ANOVA test, followed by Games-Howell test, was performed for **A** (unequal variance), and ordinary 1-way ANOVAs, following Tukey comparisons tests, were performed for **B** through **E** (equal variance). AU indicates arbitrary unit; CCL, C-C chemokine ligand; *Ccl17<sup>G/G</sup>*, *Ccl17<sup>green fluorescent protein/green fluorescent protein</sup>*; CD45<sup>+</sup>CD64<sup>+</sup>, cluster of differentiation 45 and 64 double-positive; Cxcl9, C-X-C chemokine ligand 9; DAPI, 4',6-diamidino-2-phenylindole; DT, diphtheria toxin; EMCV, encephalomyocarditis virus; *Foxp3-Dtr*, forkhead box P3–diphtheria toxin receptor; HW/BW, heart weight/body weight; IFN, interferon; *MX2*, interferon-induced GTP-binding protein MX2; NS, normal saline; *Oas2*, 2'-5'-oligoadenylate synthetase 2; RT-PCR, reverse transcription–polymerase chain reaction; Treg, regulatory T-cell; and WT, wild-type. \*\**P*<0.01 and \*\*\**P*<0.001.

expression was regulated by CSF2 signaling. More important, *Ccl17*-deficient mice displayed reduced survival, greater cardiomyocyte death and left ventricular remodeling, and increased viral load following EMCV infection. Mechanistically, we found that enhanced Treg recruitment and subsequent suppression of antiviral cytokine responses were responsible for the worsened outcomes observed in EMCV-infected *Ccl17*-deficient mice. Collectively, these findings indicate that CCL17, produced by CCR2<sup>+</sup> macrophages and dendritic cells, may represent a protective mechanism important for the host response to cardiac viral infection and suggest that CCL17 neutralization or strategies that enhance Treg recruitment early during viral myocarditis may not represent safe or effective therapies.

Expansion of tissue Tregs is a common observation reported in several studies exploring the impact of *Ccl17* deficiency across disease states.<sup>17,21,22</sup> Two mechanisms have been proposed to explain this phenomenon. In the setting of atherosclerosis, CCL17 suppressed Treg expansion by negatively impacting their differentiation and promoting apoptosis.<sup>21</sup> An alternative model is based on the finding that CCL17 and CCL22 are competitive biased ligands for their common receptor, CCR4. CCL17 and CCL22 are both expressed by CCR2<sup>+</sup> macrophages and dendritic cells and activate distinct signaling events downstream of CCR4. CCL17 activates intracellular calcium signaling, whereas CCL22 activates both  $\beta$ -arrestin and calcium signaling, each of which are important for Treg chemotaxis. When both ligands are present, CCL17 competitively inhibits CCL22-stimulated  $\beta$ -arrestin signaling and acts as a partial agonist that suppresses Treg chemotaxis.<sup>22,34</sup> These mechanisms are not mutually exclusive, and both may be relevant in myocarditis.

The exact role of Tregs in myocarditis remains controversial. Tregs may have temporal (short- versus long-term) and context-specific functions, depending on myocarditis cause (autoimmune versus viral). Tregs suppress effector cells and maintain immune

homeostasis and tolerance in various autoimmune disease models, but their role in myocarditis remains obscure.<sup>24,35–37</sup> In viral myocarditis mouse models, viral RNA and inflammation persist in the heart for several weeks and may trigger autoimmune responses.<sup>38–40</sup> Previous studies focusing on coxsackievirus B3 myocarditis suggested that transfer of exogenous Tregs or expansion of endogenous Tregs had differential effects in the short-term (promoted autoimmune responses) and long-term (protected against cardiomyopathy) phases.<sup>41–43</sup> Whether Tregs have different functions at different time points during the course of EMCV myocarditis is unknown. We identified a harmful function of Tregs at early stages of disease pathogenesis. Tregs limited interferon- $\gamma$  production, which may dampen antiviral immune responses.<sup>44</sup> Furthermore, recent discoveries highlighting the existence of functionally distinct Treg subtypes add additional complexity to this issue and raise the question of whether CCL17 might selectively influence the recruitment of particular Treg subsets.<sup>45,46</sup> These possibilities will undoubtedly be investigated in future studies.

Our study is not without limitations. We used EMCV as a model viral pathogen because EMCV causes severe disease in all mouse strains. Although unlikely, it is possible that CCL17 may have different effects on other cardiotropic viruses. Another commonly used murine viral myocarditis model is coxsackievirus B3, which produces less severe disease in many strains, except for BALB/c and A/J. It is possible CCL17 may play different roles in coxsackievirus B3–induced myocarditis. It is also important to recognize that *Ccl17* deletion most precisely models the effects of removing CCL17 during early stages of myocarditis, and our findings may not be relevant to chronic stages of myocarditis. Investigating the role of CCL17 during chronic myocarditis is clinically relevant and will require the generation of either *Ccl17<sup>fllox</sup>* mice or potent and selective CCL17 neutralizing antibodies. Nonetheless, our findings identify CCR2<sup>+</sup> macrophage- and dendritic cell–derived

CCL17 as an important mediator of the host immune response to cardiac EMCV infection and suggest that therapies that target CCL17 or enhance Treg recruitment should be avoided in acute viral myocarditis.

## CONCLUSIONS

In conclusion, we demonstrate that CCL17 protects against cardiac EMCV infection by suppressing the recruitment of Tregs and accelerating viral clearance. These findings suggest that therapeutics targeting CCL17 should be avoided in acute viral myocarditis.

## ARTICLE INFORMATION

Received October 11, 2022; accepted November 29, 2022.

### Affiliations

Cardiovascular Division, Department of Medicine (G.F., A.B., K.J.L.); and Division of Oncology (C.Z.), Washington University School of Medicine, St. Louis, MO; Department of Pathology and Immunology, Washington University, St. Louis, MO (C.-Y.L., K.J.L.); Immunology and Environment, LIMES Institute, University of Bonn, Germany (I.F.); Department of Surgery (D.K.) and Department of Developmental Biology, Washington University, St. Louis, MO (K.J.L.).

### Acknowledgments

Author contributions: Dr Feng performed the immunostaining, quantitative polymerase chain reaction, flow cytometry, and animal experiments. Dr Zhu assisted with the histology experiments. Dr Bredemeyer assisted with encephalomyocarditis virus culture. Dr Lin provided human heart tissue. Dr Förster provided the *Ccl17<sup>GFP</sup>* mice. Dr Kreisel provided *Foxp3-Dtr* mice and assisted with experimental design and critical review of the manuscript. Dr Lavine is responsible for all aspects of this manuscript, including experimental design, data analysis, and manuscript production.

### Sources of Funding

Dr Lavine is supported by grants from the National Institutes of Health (HL161185, HL150891, and HL151078), the Children's Discovery Institute (PM-LI-2019-829), Burroughs Wellcome Fund (1014782), and Leducq Foundation (20CVD02), and generous gifts through Washington University School of Medicine in St. Louis and Barnes Jewish Hospital. Dr Kreisel is supported for these studies by the National Institutes of Health (HL151685) and the Barnes-Jewish Hospital Foundation.

### Disclosures

Dr Lavine serves as a consultant for Implicit Biosciences and Medtronic and is the recipient of sponsored research agreements with Amgen and Novartis. Drs Lavine and Kreisel have a pending patent entitled "Methods for Detecting CCR2 Receptors" (application number US15/611577).

### Supplemental Material

Data S1  
Tables S1–S2  
Figures S1–S7

## REFERENCES

- Dennert R, Crijns HJ, Heymans S. Acute viral myocarditis. *Eur Heart J*. 2008;29:2073–2082. doi: 10.1093/eurheartj/ehn296
- Iwasaki A, Pillai PS. Innate immunity to influenza virus infection. *Nat Rev Immunol*. 2014;14:315–328. doi: 10.1038/nri3665
- Pollack A, Kontorovich AR, Fuster V, Dec GW. Viral myocarditis—diagnosis, treatment options, and current controversies. *Nat Rev Cardiol*. 2015;12:670–680. doi: 10.1038/nrcardio.2015.108
- Cheng C-Y, Cheng G-Y, Shan Z-G, Baritussio A, Lorenzoni G, Tyminska A, Ozieranski K, Iliceto S, Marcolongo R, Gregori D, et al. Efficacy of immunosuppressive therapy in myocarditis: a 30-year systematic review and meta analysis. *Autoimmun Rev*. 2021;20:102710. doi: 10.1016/j.autrev.2020.102710
- Heymans S, Eriksson U, Lehtonen J, Cooper LT. The quest for new approaches in myocarditis and inflammatory cardiomyopathy. *J Am Coll Cardiol*. 2016;68:2348–2364. doi: 10.1016/j.jacc.2016.09.937
- Leuschner F, Courties G, Dutta P, Mortensen LJ, Gorbатов R, Sena B, Novobrantseva TI, Borodovsky A, Fitzgerald K, Koteliansky V, et al. Silencing of CCR2 in myocarditis. *Eur Heart J*. 2015;36:1478–1488. doi: 10.1093/eurheartj/ehu225
- Miteva K, Pappritz K, El-Shafeey M, Dong F, Ringe J, Tschöpe C, Van Linthout S. Mesenchymal stromal cells modulate monocytes trafficking in coxsackievirus B3-induced myocarditis. *Stem Cells Transl Med*. 2017;6:1249–1261. doi: 10.1002/sctm.16-0353
- Cooper LT Jr, Fairweather D. *Nano-Scale Treatment for a Macro-Scale Disease: nanoparticle-Delivered siRNA Silences CCR2 and Treats Myocarditis*. Oxford University Press; 2015:1434–1436.
- Opavsky MA, Penninger J, Aitken K, Wen W-H, Dawood F, Mak T, Liu P. Susceptibility to myocarditis is dependent on the response of  $\alpha\beta$  T lymphocytes to coxsackievirus infection. *Circ Res*. 1999;85:551–558. doi: 10.1161/01.RES.85.6.551
- Klingel K, Schnorr J-J, Sauter M, Szalay G, Kandolf R.  $\beta$ 2-microglobulin-associated regulation of interferon- $\gamma$  and virus-specific immunoglobulin G confer resistance against the development of chronic coxsackievirus myocarditis. *Am J Pathol*. 2003;162:1709–1720. doi: 10.1016/S0002-9440(10)64305-2
- Hanna A, Frangogiannis NG. Inflammatory cytokines and chemokines as therapeutic targets in heart failure. *Cardiovasc Drugs Ther*. 2020;34:849–863. doi: 10.1007/s10557-020-07071-0
- Chen B, Frangogiannis NG. Chemokines in myocardial infarction. *J Cardiovasc Transl Res*. 2021;14:35–52. doi: 10.1007/s12265-020-10006-7
- Mizukami Y, Kono K, Kawaguchi Y, Akaike H, Kamimura K, Sugai H, Fujii H. CCL17 and CCL22 chemokines within tumor microenvironment are related to accumulation of Foxp3+ regulatory T cells in gastric cancer. *Int J Cancer*. 2008;122:2286–2293. doi: 10.1002/ijc.23392
- Tsunemi Y, Saeki H, Nakamura K, Nagakubo D, Nakayama T, Yoshie O, Kagami S, Shimazu K, Kadono T, Sugaya M, et al. CCL17 transgenic mice show an enhanced Th2-type response to both allergic and non-allergic stimuli. *Eur J Immunol*. 2006;36:2116–2127. doi: 10.1002/eji.200535564
- Staples KJ, Hinks TS, Ward JA, Gunn V, Smith C, Djukanović R. Phenotypic characterization of lung macrophages in asthmatic patients: overexpression of CCL17. *J Allergy Clin Immunol*. 2012;130:1404–1412. e1407.
- Riis JL, Johansen C, Vestergaard C, Bech R, Kragballe K, Iversen L. Kinetics and differential expression of the skin-related chemokines CCL27 and CCL17 in psoriasis, atopic dermatitis and allergic contact dermatitis. *Exp Dermatol*. 2011;20:789–794. doi: 10.1111/j.1600-0625.2011.01323.x
- Heiseke AF, Faul AC, Lehr HA, Förster I, Schmid RM, Krug AB, Reindl W. CCL17 promotes intestinal inflammation in mice and counteracts regulatory T cell-mediated protection from colitis. *Gastroenterology*. 2012;142:335–345. doi: 10.1053/j.gastro.2011.10.027
- Radstake TR, van der Voort R, ten Brummelhuis M, de Waal MM, Looman M, Figdor C, van den Berg W, Barrera P, Adema G, et al. Increased expression of CCL18, CCL19, and CCL17 by dendritic cells from patients with rheumatoid arthritis, and regulation by Fc gamma receptors. *Ann Rheum Dis*. 2005;64:359–367. doi: 10.1136/ard.2003.017566
- Lee M-C, Saleh R, Achuthan A, Fleetwood AJ, Förster I, Hamilton JA, Cook AD. CCL17 blockade as a therapy for osteoarthritis pain and disease. *Arthritis Res Ther*. 2018;20:1–10.
- Achuthan A, Cook AD, Lee M-C, Saleh R, Khiew H-W, Chang MW, Louis C, Fleetwood AJ, Lacey DC, Christensen AD, et al. Granulocyte macrophage colony-stimulating factor induces CCL17 production via IRF4 to mediate inflammation. *J Clin Invest*. 2016;126:3453–3466. doi: 10.1172/JCI87828
- Weber C, Meiler S, Döring Y, Koch M, Drechsler M, Megens RT, Rowinska Z, Bidzhekov K, Fecher C, Ribechini E, et al. CCL17-expressing dendritic cells drive atherosclerosis by restraining regulatory T cell homeostasis in mice. *J Clin Invest*. 2011;121:2898–2910. doi: 10.1172/JCI44925
- Feng G, Bajpai G, Ma P, Koenig A, Bredemeyer A, Lokshina I, Lai L, Förster I, Leuschner F, Kreisel D, et al. CCL17 aggravates myocardial injury by suppressing recruitment of regulatory T-cells. *Circulation*. 2022;145:765–782. doi: 10.1161/CIRCULATIONAHA.121.055888
- Alferink J, Lieberam I, Reindl W, Behrens A, Weiß S, Hüser N, Gerauer K, Ross R, Reske-Kunz AB, Ahmad-Nejad P, et al. Compartmentalized production of CCL17 in vivo: strong inducibility in peripheral

- dendritic cells contrasts selective absence from the spleen. *J Exp Med*. 2003;197:585–599. doi: [10.1084/jem.20021859](https://doi.org/10.1084/jem.20021859)
24. Kim JM, Rasmussen JP, Rudensky AY. Regulatory T cells prevent catastrophic autoimmunity throughout the lifespan of mice. *Nat Immunol*. 2007;8:191–197. doi: [10.1038/ni1428](https://doi.org/10.1038/ni1428)
  25. Satpathy AT, Kc W, Albring JC, Edelson BT, Kretzer NM, Bhattacharya D, Murphy TL, Murphy KM. Zbtb46 expression distinguishes classical dendritic cells and their committed progenitors from other immune lineages. *J Exp Med*. 2012;209:1135–1152. doi: [10.1084/jem.20120030](https://doi.org/10.1084/jem.20120030)
  26. Clemente-Casares X, Hosseinzadeh S, Barbu I, Dick SA, Macklin JA, Wang Y, Momen A, Kantores C, Aronoff L, Farno M, et al. A CD103+ conventional dendritic cell surveillance system prevents development of overt heart failure during subclinical viral myocarditis. *Immunity*. 2017;47:974–989. doi: [10.1016/j.immuni.2017.10.011](https://doi.org/10.1016/j.immuni.2017.10.011)
  27. Ruland C, Renken H, Kuzmanov I, Mehr AF, Schwarte K, Cerina M, Herrmann A, Otte D-M, Zimmer A, Schwab N, et al. Chemokine CCL17 is expressed by dendritic cells in the CNS during experimental autoimmune encephalomyelitis and promotes pathogenesis of disease. *Brain Behav Immun*. 2017;66:382–393. doi: [10.1016/j.bbi.2017.06.010](https://doi.org/10.1016/j.bbi.2017.06.010)
  28. Bajpai G, Schneider C, Wong N, Bredemeyer A, Hulsmans M, Nahrendorf M, Epelman S, Kreisel D, Liu Y, Itoh A, et al. The human heart contains distinct macrophage subsets with divergent origins and functions. *Nat Med*. 2018;24:1234–1245. doi: [10.1038/s41591-018-0059-x](https://doi.org/10.1038/s41591-018-0059-x)
  29. Mariani M, Lang R, Binda E, Panina-Bordignon P, D'Ambrosio D. Dominance of CCL22 over CCL17 in induction of chemokine receptor CCR4 desensitization and internalization on human Th2 cells. *Eur J Immunol*. 2004;34:231–240. doi: [10.1002/eji.200324429](https://doi.org/10.1002/eji.200324429)
  30. Baatar D, Olkhanud P, Sumitomo K, Taub D, Gress R, Biragyn A. Human peripheral blood T regulatory cells (Tregs), functionally primed CCR4+ Tregs and unprimed CCR4– Tregs, regulate effector T cells using FasL. *J Immunol*. 2007;178:4891–4900. doi: [10.4049/jimmunol.178.8.4891](https://doi.org/10.4049/jimmunol.178.8.4891)
  31. Magnani JW, Dec GW. Myocarditis: current trends in diagnosis and treatment. *Circulation*. 2006;113:876–890. doi: [10.1161/CIRCULATIONAHA.105.584532](https://doi.org/10.1161/CIRCULATIONAHA.105.584532)
  32. Kania G, Siegert S, Behnke S, Prados-Rosales R, Casadevall A, Lüscher TF, Luther SA, Kopf M, Eriksson U, Blyszczuk P, et al. Innate signaling promotes formation of regulatory nitric oxide-producing dendritic cells limiting T-cell expansion in experimental autoimmune myocarditis. *Circulation*. 2013;127:2285–2294. doi: [10.1161/CIRCULATIONAHA.112.000434](https://doi.org/10.1161/CIRCULATIONAHA.112.000434)
  33. Rose NR. Viral myocarditis. *Curr Opin Rheumatol*. 2016;28:383–389. doi: [10.1097/BOR.0000000000000303](https://doi.org/10.1097/BOR.0000000000000303)
  34. Anderson CA, Solari R, Pease JE. Biased agonism at chemokine receptors: obstacles or opportunities for drug discovery? *J Leukoc Biol*. 2016;99:901–909. doi: [10.1189/jlb.2MR0815-392R](https://doi.org/10.1189/jlb.2MR0815-392R)
  35. Pandiyan P, Zheng L, Ishihara S, Reed J, Lenardo MJ. CD4+ CD25+ Foxp3+ regulatory T cells induce cytokine deprivation-mediated apoptosis of effector CD4+ T cells. *Nat Immunol*. 2007;8:1353–1362. doi: [10.1038/ni1536](https://doi.org/10.1038/ni1536)
  36. Kleinewietfeld M, Hafler DA. The plasticity of human Treg and Th17 cells and its role in autoimmunity. *Semin Immunol*. 2013;25:305–312. doi: [10.1016/j.smm.2013.10.009](https://doi.org/10.1016/j.smm.2013.10.009)
  37. Cvetanovich GL, Hafler DA. Human regulatory T cells in autoimmune diseases. *Curr Opin Immunol*. 2010;22:753–760. doi: [10.1016/j.coi.2010.08.012](https://doi.org/10.1016/j.coi.2010.08.012)
  38. Rose NR. Myocarditis: infection versus autoimmunity. *J Clin Immunol*. 2009;29:730–737. doi: [10.1007/s10875-009-9339-z](https://doi.org/10.1007/s10875-009-9339-z)
  39. Huber S, Gauntt C, Sakkinen P. Enteroviruses and myocarditis: viral pathogenesis through replication, cytokine induction, and immunopathogenicity. *Adv Virus Res*. 1998;51:35–80b.
  40. Klingel K, Hohenadl C, Canu A, Albrecht M, Seemann M, Mall G, Kandolf R. Ongoing enterovirus-induced myocarditis is associated with persistent heart muscle infection: quantitative analysis of virus replication, tissue damage, and inflammation. *Proc Natl Acad Sci*. 1992;89:314–318. doi: [10.1073/pnas.89.1.314](https://doi.org/10.1073/pnas.89.1.314)
  41. Xie Y, Chen R, Zhang X, Chen P, Liu X, Xie Y, Yu Y, Yang Y, Zou Y, Ge J, et al. The role of Th17 cells and regulatory T cells in Coxsackievirus B3-induced myocarditis. *Virology*. 2011;421:78–84. doi: [10.1016/j.virol.2011.09.006](https://doi.org/10.1016/j.virol.2011.09.006)
  42. Huber SA, Feldman AM, Sartini D. Coxsackievirus B3 induces T regulatory cells, which inhibit cardiomyopathy in tumor necrosis factor- $\alpha$  transgenic mice. *Circ Res*. 2006;99:1109–1116. doi: [10.1161/01.RES.0000249405.13536.49](https://doi.org/10.1161/01.RES.0000249405.13536.49)
  43. Pappritz K, Savvatis K, Miteva K, Kerim B, Dong F, Fechner H, Müller I, Brandt C, Lopez B, González A, et al. Immunomodulation by adoptive regulatory T-cell transfer improves coxsackievirus B3-induced myocarditis. *FASEB J*. 2018;32:6066–6078. doi: [10.1096/fj.201701408F](https://doi.org/10.1096/fj.201701408F)
  44. Sojka DK, Fowell DJ. Regulatory T cells inhibit acute IFN- $\gamma$  synthesis without blocking T-helper cell type 1 (Th1) differentiation via a compartmentalized requirement for IL-10. *Proc Natl Acad Sci*. 2011;108:18336–18341. doi: [10.1073/pnas.1110566108](https://doi.org/10.1073/pnas.1110566108)
  45. Herrnstadt G, Steinmetz O. The role of treg subtypes in glomerulonephritis. *Cell Tissue Res*. 2021;385:293–304. doi: [10.1007/s00441-020-03359-7](https://doi.org/10.1007/s00441-020-03359-7)
  46. Amarillo D, Brugnini A, Trías N, Rodríguez Sande V, Salisbury S, Cuello M, Lens D. Circulating T regulatory cell subsets in patients with untreated lung cancer. *Clin Transl Oncol*. 2022;24:1755–1763.

## **SUPPLEMENTAL MATERIAL**



## **Data S1. Expanded Materials and Methods**

**Human Studies.** Myocardial tissue was obtained from donor control and heart failure patients following left ventricular assist device implantation or heart transplantation. The study was approved by the Washington University Institutional Review Board (Study# 201104172). Paraffin-embedded sections of lymphocytic myocarditis, Covid-19 myocardium and donor heart tissue were dewaxed in xylene, and rehydrated. Opal™ 4-Color Manual IHC Kit (PerkinElmer, Cat# NEL810001KT) was used for the staining. Slide preparation, microwave treatment, blocking, primary antibody incubation (CCL17, Abcam, Cat#ab195044; CD68, Biorad, MCA5709), introduction of secondary-HRP, opal signal generation, counterstain and mount were performed as instructed.

**Animal Studies.** Mice were bred and maintained at the Washington University School of Medicine and all experimental procedures were done in accordance with the animal use oversight committee. All *Ccl17<sup>Gfp</sup>*, *Foxp3-Dtr*, *Ccr2<sup>ErCre</sup>*, *Rosa26* *Tdtomato*, *Ccr2<sup>-/-</sup>*, *Csf2rb<sup>flox/flox</sup>* and *Zbtb46<sup>Gfp</sup>* mice were on the C57/B6J background and genotyped according to established protocols. Equal numbers of male and female mice at same age (8-12 weeks) were included in all experiments. Mice were infected with 10<sup>4</sup> PFU EMCV-D to establish acute viral myocarditis model. Mice were monitored for survival and survived mice were sacrificed for further analysis.

**Flow cytometry.** To generate single cell suspensions, saline perfused hearts were finely minced and digested in Dulbecco's Modified Eagle Medium (DMEM, Gibco) with collagenase I (450 U/ml, Sigma CAS# 9001-12-1), hyaluronidase (60 U/ml, Sigma CAS# 37326-33-3) and DNase I (60 U/ml, Sigma CAS# 9003-98-9) for 45 minutes at 37°C. All enzymes were purchased from Sigma. To deactivate the enzymes, samples were washed with Hanks' Balanced Salt Solution (Gibco, HBSS) that was supplemented with 2% Fetal Bovine Serum (Sigma, FBS) and 0.2% Bovine Serum Albumin (Sigma, BSA, cas#9048-46-8) and filtered through 40 µm cell strainers. Red blood cell lysis was performed with ACK lysis buffer (Thermo Fisher Scientific, cat# A1049201). Samples were washed with HBSS and resuspended in 100 µL FACS

buffer which is PBS with 2% FBS and 2 mM EDTA (CORNING, Product# 46-034-CI). To check the expressions of surface markers, cells were stained with monoclonal antibodies at 4°C for 30 minutes in the dark. To check the expressions of intracellular marker like Foxp3 and IFN- $\gamma$ , cells were fixed and permeabilized using a True-Nuclear™ Transcription Factor Buffer Set (BIOLEGEND, cat# 424401) before staining with Foxp3 and IFN- $\gamma$  antibodies for 30 minutes. Specially for IFN- $\gamma$  staining, mice were injected with 200  $\mu$ g protein transport inhibitor brefeldin A (BIOLEGEND, cat#420601) to enhance intracellular cytokine staining signals 4-6 hours before sacrifice. All the antibodies were obtained from BIOLEGEND. A complete list of antibodies is provided below. Samples were washed twice, and final resuspension was made in 300  $\mu$ L FACS buffer. Isotype control antibodies were used to validate our flow cytometry gating strategy. Flow cytometric analysis and sorting were performed on BD LSRII and BD FACSMelody platforms, respectively.

CD45-PerCP/Cy5.5, clone 30-F11 (BIOLEGEND cat# 103131)

CD64-APC and PE, clone X54-5/7.1 (BIOLEGEND cat# 139305, 139303)

LY6C-APC, PE and FITC, clone HK1.4 (BIOLEGEND cat# 128007, 128015, 128005)

CCR2-BV421, clone: SA203G11 (BIOLEGEND cat# 150605)

MHCII-APC/Cy7, clone M5/114.15.2 (BIOLEGEND cat# 107627)

LY6G-PE/Cy7 and FITC, clone 1A8 (BIOLEGEND cat# 127617, 127605)

CD3-FITC, APC and PE, clone 17A2 (BIOLEGEND cat#100203, 100235, 100205)

CD4-FITC and BV510, clone RM4-5 (BIOLEGEND cat#100509, 100553)

CD8-PE/Cy7, clone 53-6.7 (BIOLEGEND cat# 100721)

CD25-APC/Cy7, clone 3C7 (BIOLEGEND cat# 101917)

CD44-APC, clone IM7 (BIOLEGEND cat#103011)

CD62L-PE, clone MEL-14 (BIOLEGEND cat#104408)

CD69-PerCP/Cy5.5 and BV510, clone H1.2F3 (BIOLEGEND cat#104521, 104531)

FOXP3-BV421, clone MF-14 (BIOLEGEND cat# 126419)

CD19-PE, clone 6D5 (BIOLEGEND cat# 115507).

CD11b-PE and PE/Cy7, clone M1/70 (BIOLEGEND cat# 101207, 101215)

CX3CR1-FITC and APC/CY7, clone SA011F11 (BIOLEGEND cat# 149020)

IFN- $\gamma$ -PE, clone MOB-47 (BIOLEGEND cat# 113603)

**Trichrome staining and wheat germ agglutinin (WGA) staining.** Mouse hearts were fixed in 4% paraformaldehyde solution (fisher scientific, cat#50-980-495) overnight at 4°C, dehydrated in 70% ethyl alcohol, and embedded in paraffin. 6- $\mu$ m sections were cut and slides were dewaxed and rehydrated following standard histochemistry protocol. To assess cardiac fibrosis, trichrome staining (Thermo Scientific, Advanced Testing Gomori's Trichrome Stain kit, Product# 10076248) was performed using standard techniques and quantified using Image J software. To quantify cardiomyocyte cross-sectional area, paraffin sections were stained with rhodamine conjugated WGA (Vector labs, Cat# RL-1022), visualized on a Zeiss confocal microscope, and measurements performed using Zeiss Axiovision software.

**Mouse heart tissue immunostaining.** For mouse heart tissue immunostaining assays, tissues were fixed in 4% paraformaldehyde overnight at 4°C, infiltrated with 30% sucrose (Sigma, CAS# 57-50-1), embedded in embedding medium for frozen tissue specimens to ensure Optimal Cutting Temperature O.C.T. compound (SAKURA, Product# 4583), frozen and 6- $\mu$ m cryosections cut. Tissue was blocked by 5% FBS for 30 minutes before primary antibodies incubation with GFP (Abcam, Cat# ab13970), CD68 clone FA-11 (BIOLEGEND, Cat# 137001), CD4 (Abcam, cat#183685), and Foxp3 (cell signaling technology, cat#12653) antibodies. For the intracellular Foxp3 staining, tissues were permeabilized with 0.25% triton 100 (Invitrogen, cat# HFH10) for 5 minutes before Foxp3 antibody incubation. Immunofluorescence was visualized using appropriate secondary antibodies on a Zeiss confocal microscopy system. Antibody specificity was validated using appropriate no primary and isotype controls. CD68<sup>+</sup> macrophages and GFP-CCL17<sup>+</sup> cells were quantified by examining at least 4 similarly oriented sections from 4 independent samples in blinded fashion.

**In Situ Cardiomyocyte Death Detection.** To detect mouse cardiomyocyte death following EMCV infection, a TMR red In Situ Cell Death Detection Kit (sigma, cat#

12156792910) was used. Labeling of DNA strand breaks by Terminal deoxynucleotidyl transferase (TdT) which catalyzes polymerization of labeled nucleotides to free 3'-OH DNA ends in a template-independent manner (TUNEL-reaction). TMR red labeled nucleotides, incorporated in nucleotide polymers, are detected and quantified by fluorescence microscopy or flow cytometry. Frozen slides of mouse hearts were blocked with 5% FBS following by overnight incubation of cardiac troponin I (abcam, cat# ab47003) at 4°C and appropriate secondary antibody for 30 minutes at room temperature to visualize cardiomyocyte staining. After 3 washes with PBS, slides were incubated with the TUNEL reaction mixture in humidified chamber (wet Kimwipes) at 37°C for 60 minutes. Slides were washed 3 times with TBST before mounting with antifade mounting medium with DAPI (Vector Laboratories, cat# H-1200).

**RNA extraction and quantitative real-time RT-PCR.** Total RNA was from hearts and sorted cells isolated using the TRIzol reagent (Thermo Fisher Scientific, cat#15596026) and purified with a PureLink™ Mini kit (Thermo Fisher Scientific, cat#12183025), then cDNA was synthesized from total RNA with High Capacity cDNA Reverse Transcriptase kit (Thermo Fisher Scientific, cat# 4368813) according to the manufacturer's instructions. Gene expression was measured by the change-in-threshold ( $\Delta\Delta CT$ ) method based on quantitative real-time PCR in a QuantStudio 3 machine (Applied Biosystems) with SYBR reagent (Thermo Fisher Scientific, cat#4309155) and the following primers for mouse genes.

**Statistical analysis.** Statistical analysis was performed with Prism 8 (GraphPad Software). Data were analyzed for normal distribution by Shapiro-Wilk normality test. F test (two groups comparisons) and Brown-Forsythe test (multiple groups comparisons) were used to test the equality of variances. Unpaired t test was performed for two group comparisons with equal variance. Unpaired t test with Welch's correction was performed for two group comparisons with unequal variance. Ordinary one-way ANOVA followed by Games-Howell's test (comparing each group with every other group) was performed for multiple comparisons (one experimental

factor) with equal group variance. Brown-Forsythe and Welch ANOVA followed by Games-Howell's test (comparing each group with every other group) was performed for comparisons (one experimental factor) with unequal group variance. For all the other data, P value represented significance were labeled on the figures.

**Data Availability.** Source Data for all experiments are provided and available from the corresponding author on reasonable request.

**Table S1. Mouse primer sequence for qRT-PCR**

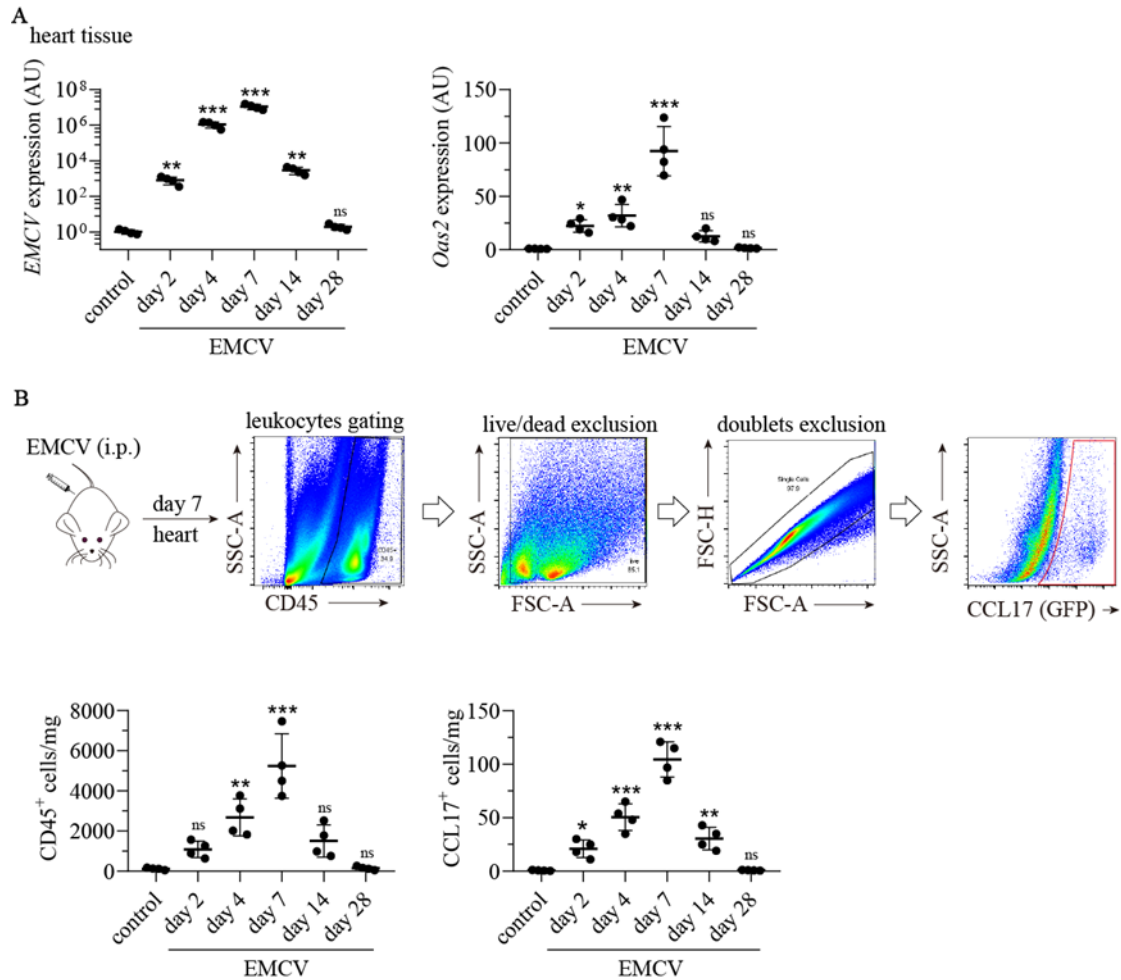
ID	mouse primer sequence
Emcv-forward	GTCGTGAAGGAAGCAGTTCCTC
Emcv-reverse	CACGTGGCTTTTGGCCGCAGAGG
Oas2-forward	GCCTGAATACTGAGTCACCTG
Oas2-reverse	TTCAGTAAGTGGCTTGGAGTG
Mx2-forward	ACCAGAGTGCAAGTGAGGAGCT
Mx2-reverse	GTA CTAGGGCAGTGATGTCCTG
Cxcl9-forward	AGTCCGCTGTTCTTTTCCTC
Cxcl9-reverse	TGAGGTCTTTGAGGGATTTGTAG
Cxcl10-forward	TCAGCACCATGAACCCAAG
Cxcl10-reverse	CTATGGCCCTCATTCTCACTG
Ifn $\alpha$ 1-forward	TCTGTGCTTTCCTGATGGTC
Ifn $\alpha$ 1-reverse	GGTTATGAGTCTGAGGAAGGTC
Ifn $\alpha$ 2-forward	GAGAGAAGAAACACAGCCCC
Ifn $\alpha$ 2-reverse	AGCAAGTTGACTGAGGAAGAC
Ifn $\beta$ 1-forward	CGAGCAGAGATCTTCAGGAAC
Ifn $\beta$ 1-reverse	TCACTACCAGTCCCAGAGTC
Ifn $\gamma$ -forward	CTTTGGACCCTCTGACTTGAG
Ifn $\gamma$ -reverse	TCAATGACTGTGCCGTGG
Tnf $\alpha$ -forward	GATCTCAAAGACAACCAACATGTG
Tnf $\alpha$ -reverse	CTCCAGCTGGAAGACTCCTCCCAG
Il1 $\beta$ -forward	ACGGACCCCAAAGATGAAG
Il1 $\beta$ -reverse	TTCTCCACAGCCACAATGAG
Ccl3-forward	GATTCCACGCCAATTCATCG
Ccl3-reverse	TTCAGTTCCAGGTCAGTGATG
Ccl4-forward	TGACCAAAGAGGCAGACAG
Ccl4-reverse	GTGAGAAGCATCAGGGCTG
Ccl9-forward	AACTGCTCTTGGAATCTGGG
Ccl9-reverse	GTGAGTTATAGGACAGGCAGC

**Table S2. Information of Covid-19 infected patients**

	Age (years)	sex	ARDS	Cause of death/procurement	EF (%)	Troponin I (ng/mL)
Donor-1	56	M	no	explant	21	NA
Donor-2	38	F	no	explant	68	NA
Donor-3	53	F	no	explant	63	NA
Donor-4	54	F	no	explant	57	NA
Donor-5	65	F	no	explant	60	NA
Donor-6	62	M	no	explant	74	NA
LM-1	29	M	no	right bundle branch block	NA	NA
LM-2	1	M	no	ventricular tachycardia	NA	NA
LM-3	13	M	no	coronary spasm	NA	NA
LM-4	44	F	no	cardiogenic shock	NA	NA
LM-5	1	F	no	unspecific cardiomyopathy	NA	NA
Covid19-1	61	M	yes	cardiac arrest	<30	7.457
Covid19-2	54	M	yes	cardiac arrest	45	10.94
Covid19-3	62	F	yes	cardiac arrest	30	37.77
Covid19-4	22	F	yes	cardiac arrest	40	6.49
Covid19-5	61	M	yes	cardiac arrest	NA	NA

ARDS: acute respiratory distress syndrome, EF: ejection fraction, LM: lymphocytic myocarditis, M: male, F: female, NA: not available.

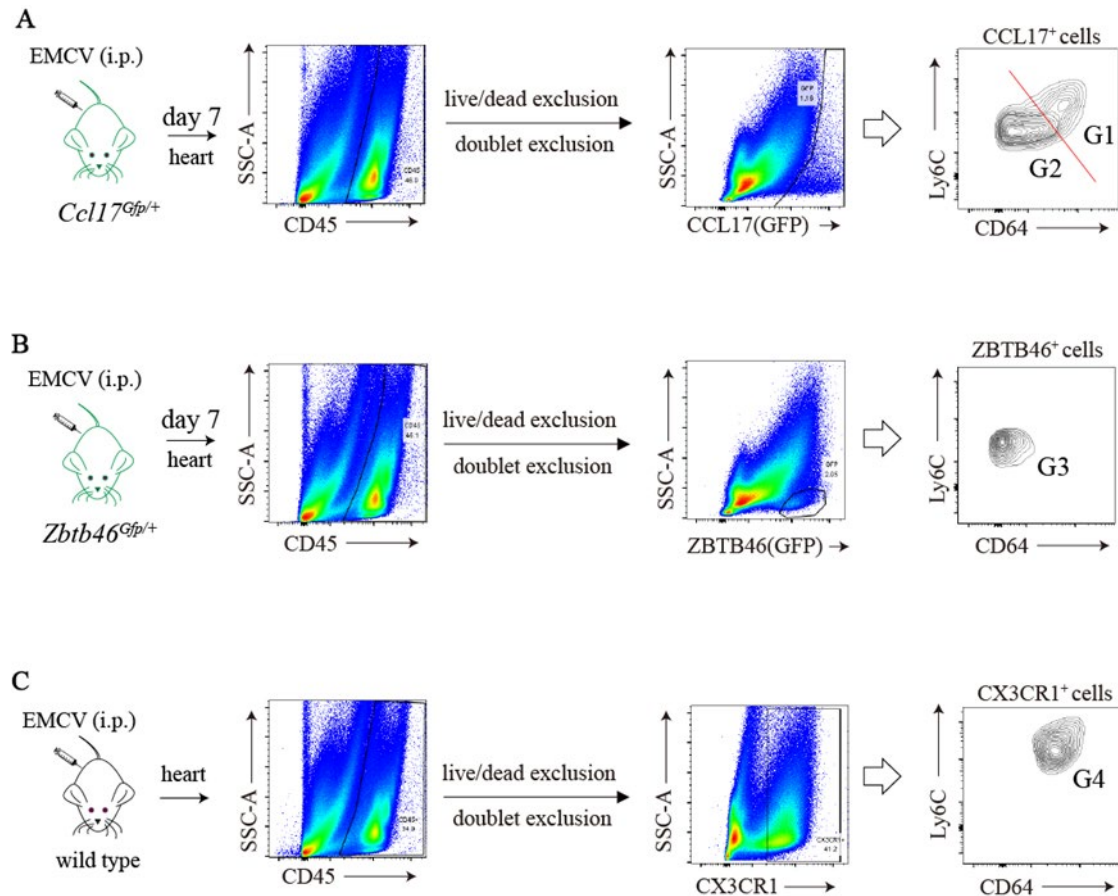
**Figure S1.** Expressions of *Emcv* and *Oas2* in wild type mouse hearts and flow cytometric analysis of CD45<sup>+</sup> and CCL17<sup>+</sup> cells in wild type mouse hearts.



Expressions of *EMCV* and *Oas2* in wild type heart and flow cytometry gating strategies for CD45<sup>+</sup> and CCL17<sup>+</sup> cells. **A**, Quantitative RT-PCR (Reverse Transcription Polymerase Chain Reaction) measuring mRNA levels of encephalomyocarditis viruses (*Emcv*) and 2'-5'-oligoadenylate synthetase 2 (*Oas2*) in hearts of wild type mice 2, 4, 7, 14 and 28 days after EMCV infection. N=4 per experimental group. **B**, Flow cytometry gating scheme to identify green fluorescent protein (GFP)<sup>+</sup> CCL17 expressing immune cells from hearts of *Ccl17<sup>Gfp/+</sup>* mice that underwent saline injection (control) and EMCV injection. All data are mean  $\pm$  SD and presented normality. Welch ANOVA followed by Games-Howell's tests for **A** (unequal variance) and ordinary one-way ANOVA following Tukey's multiple comparisons tests for **B** (equal variance) were performed. For all data, "ns" indicate non-significance, \* indicate  $P < 0.05$ , \*\* indicate  $P < 0.01$ , and \*\*\* indicate  $P < 0.001$ .

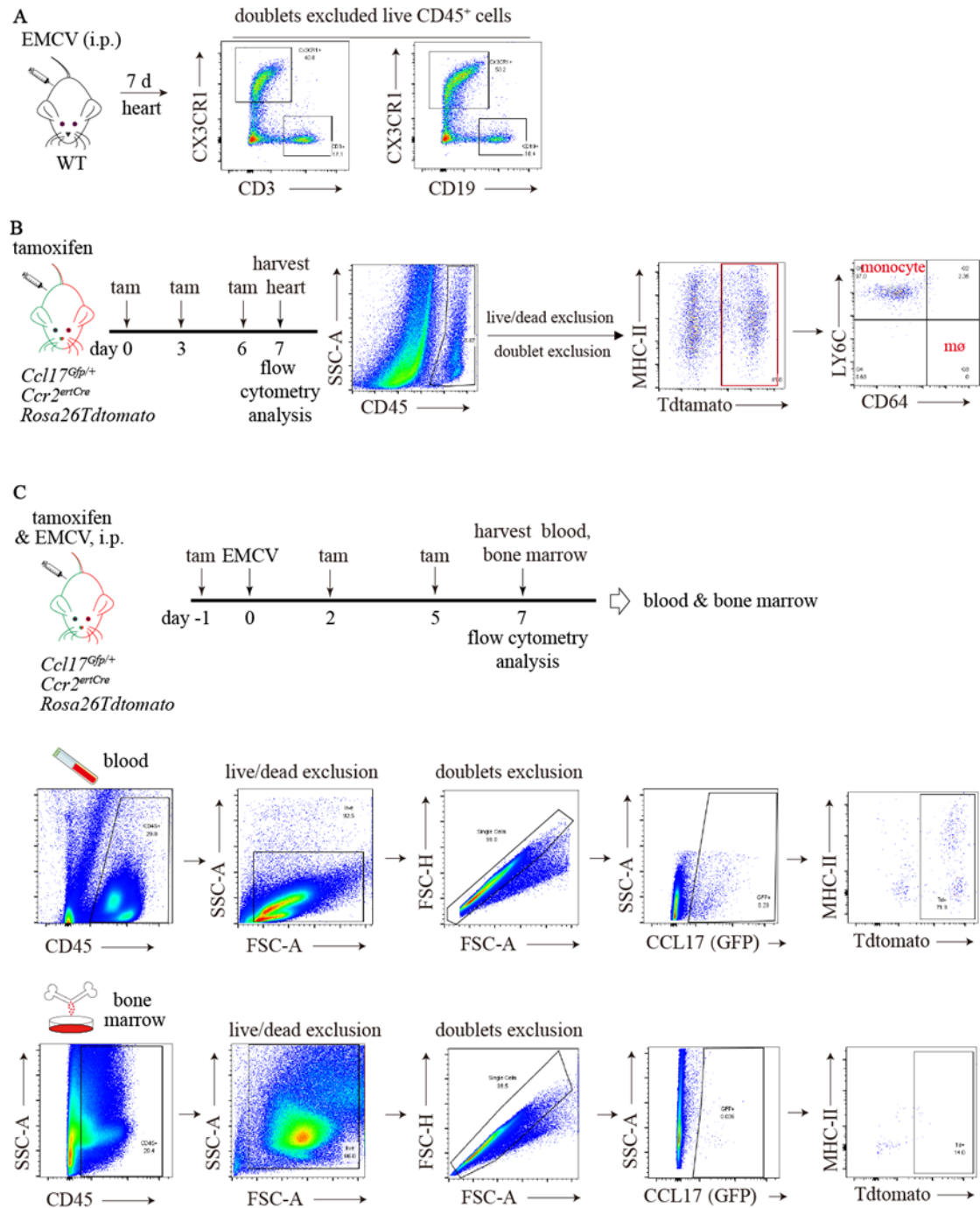


**Figure S2.** Flow cytometry gating strategies of G1/G2 CCL17<sup>+</sup> cells in *Ccl17*<sup>Gfp/+</sup> mouse hearts, G3 ZBTB46<sup>+</sup> dendritic cells in *Zbtb46*<sup>Gfp/+</sup> mouse hearts and G4 CD64<sup>+</sup> macrophages in wild type mouse hearts following.



Flow cytometry gating strategies of G1/G2 CC chemokine ligand 17 (CCL17)<sup>+</sup> cells (A) in *Ccl17*<sup>green fluorescent protein/+</sup> (*Ccl17*<sup>Gfp/+</sup>) mouse hearts, G3 ZBTB46<sup>+</sup> dendritic cells (B) in *Zinc Finger And BTB Domain Containing 46* (*Zbtb46*)<sup>Gfp/+</sup> mouse hearts and G4 cluster of differentiation 64 (CD64)<sup>+</sup> macrophages (C) in wild type mouse hearts following 7 days encephalomyocarditis viruses (EMCV) infection. For A, B and C, 4 mice in each group were treated identically, and hearts were harvested on the same day in one experiment to make the comparisons parallelly.

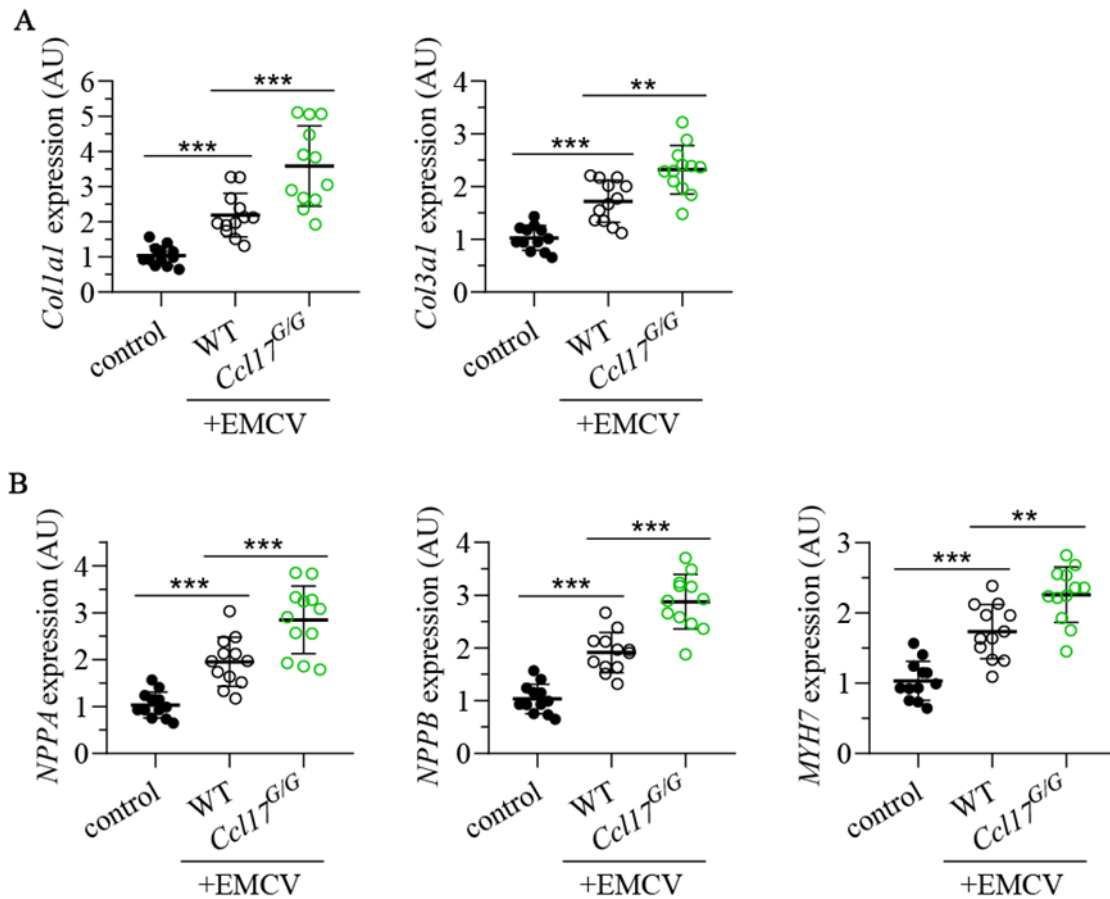
**Figure S3. A.** Flow cytometry confirms CX3CR1 as myeloid cell marker which exclude CD3 and CD19 expression. **B.** Flow cytometry showing Tdtomato positive cells properties. **C.** Flow cytometry showing CCR2 expression in CCL17<sup>+</sup> cells of blood and bone marrow.



Myeloid cell gating strategy and C-C chemokine receptor type 2 (CCR2) expression in CC chemokine ligand 17 (CCL17)<sup>+</sup> cells of blood and bone marrow. **A.** Flow cytometry confirms cx3c chemokine receptor type 1 (CX3CR1) as myeloid cell marker which exclude cluster of differentiation (CD3) and CD19 expression. **B.** Flow

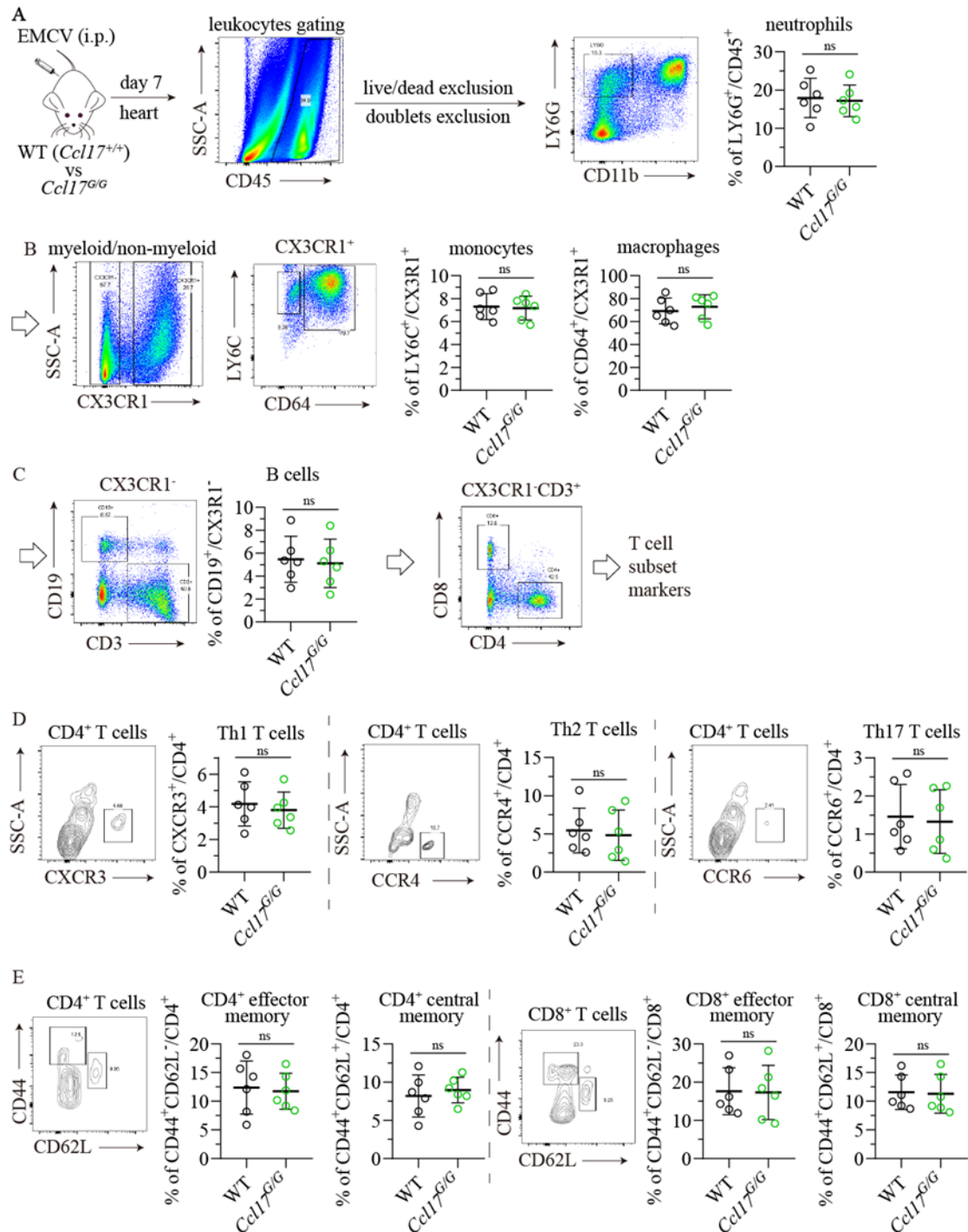
cytometry showing Tdtomato positive cells properties. **C.** Flow cytometry showing CCR2 expression in CCL17<sup>+</sup> cells of blood and bone marrow. N=4 per experimental group.

**Figure S4.** Effects of *Ccl17* deficiency on cardiac fibrosis and hypertrophy.



Effects of *Ccl17* deficiency on cardiac fibrosis marked by collagen 1a1&3a1 (A) and hypertrophy marked by Natriuretic Peptide A&B (NPPA&B), myosin heavy chain 7 (MYH7; B) checked by qRT-PCR 14 days following EMCV infection. For A and B, wild type (*Ccl17*<sup>+/+</sup>) mice were injected with saline as control, wild type (*Ccl17*<sup>+/+</sup>) and *Ccl17* deficient (*Ccl17*<sup>green fluorescent protein / green fluorescent protein</sup>, abbreviated as *Ccl17*<sup>G/G</sup>) were injected with EMCV as model groups. The survived mice were sacrificed on day 14 and hearts were harvested for qRT-PCR. For multiple comparisons didn't present normality (A/*Coll1a1* and B/*NPPA*), nonparametric Kruskal-Wallis tests were performed. For other multiple comparisons presented normality and showed equal variance (A/*Col3a1* and B/*NPPB*/*MYH7*), ordinary one-way ANOVA following Tukey's multiple comparisons tests were performed. For all data, \*\* indicate  $P < 0.01$ , and \*\*\* indicate  $P < 0.001$ .

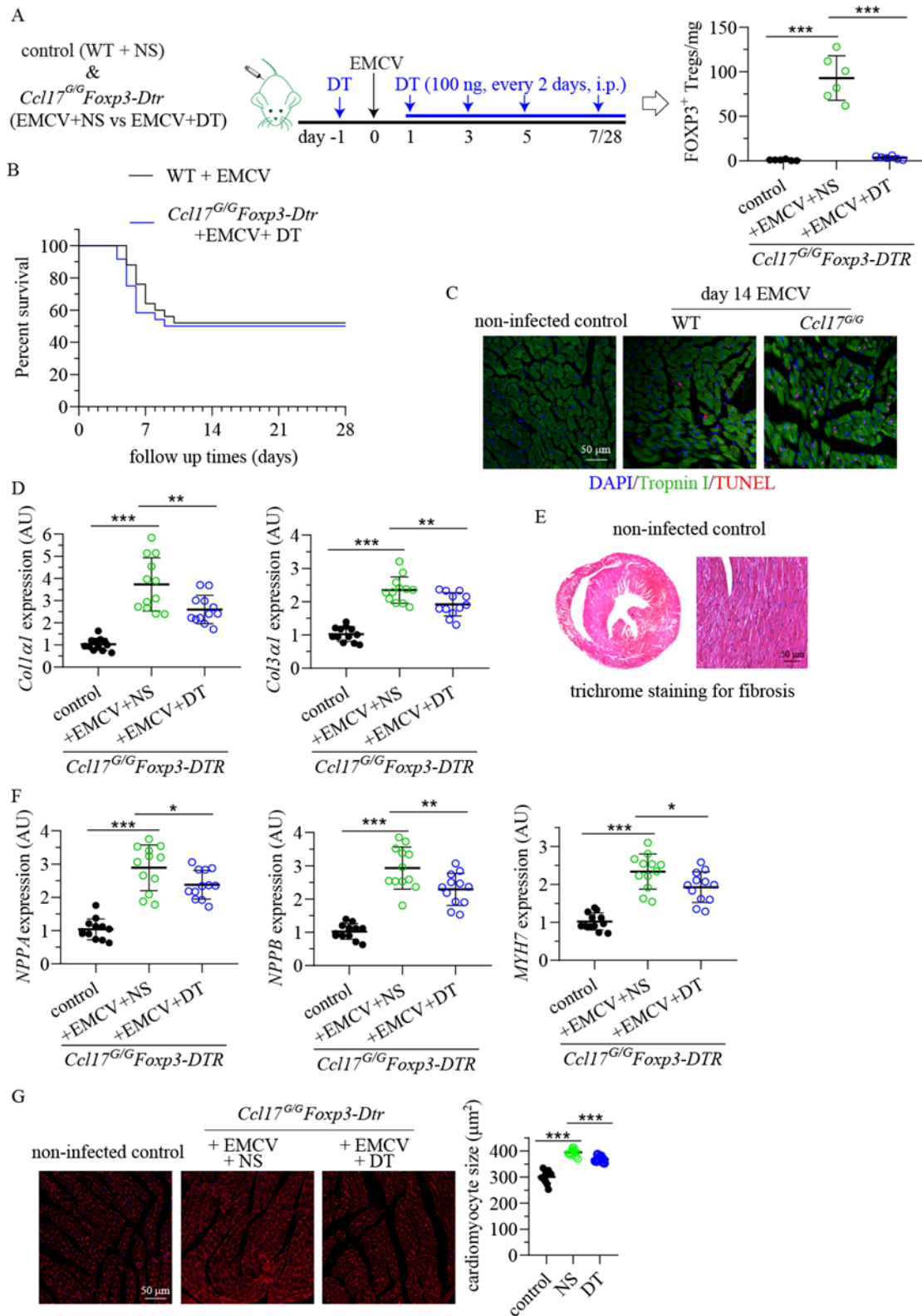
**Figure S5.** Effects of *Ccl17* deficiency on cardiac leukocyte abundance following EMCV infection.



Effects of CC chemokine ligand 17 (*Ccl17*) deficiency on cardiac leukocyte abundance following encephalomyocarditis viruses (EMCV) infection. Cardiac leukocyte abundance following EMCV infection. Proportion of Lymphocyte antigen 6 complex locus G (LY6G)<sup>+</sup> neutrophils (A), lymphocyte antigen 6 complex locus C (LY6C)<sup>+</sup> monocytes (B), cluster of differentiation 64 (CD64)<sup>+</sup> macrophages (B), and T cell subsets including Th1, Th2, Th7, CD4<sup>+</sup> effector memory T cells, CD4<sup>+</sup> central memory

T cells, CD8<sup>+</sup> effector memory T cells and CD8<sup>+</sup> central memory T cells (C-E) were analyzed by flow cytometry 7 days after EMCV infection. For A-E, wild type (*Ccl17*<sup>+/+</sup>) and *Ccl17* deficient (*Ccl17*<sup>green fluorescent protein / green fluorescent protein</sup>, abbreviated as *Ccl17*<sup>GG</sup>) were injected with EMCV as experimental groups. N=6 per experimental group. All data are mean ± SD and presented normality. All data showed equal variance. Unpaired t tests were performed, and “ns” indicate non-significance.

**Figure S6.** Effect of Treg depletion on survival rate and heart remodeling.

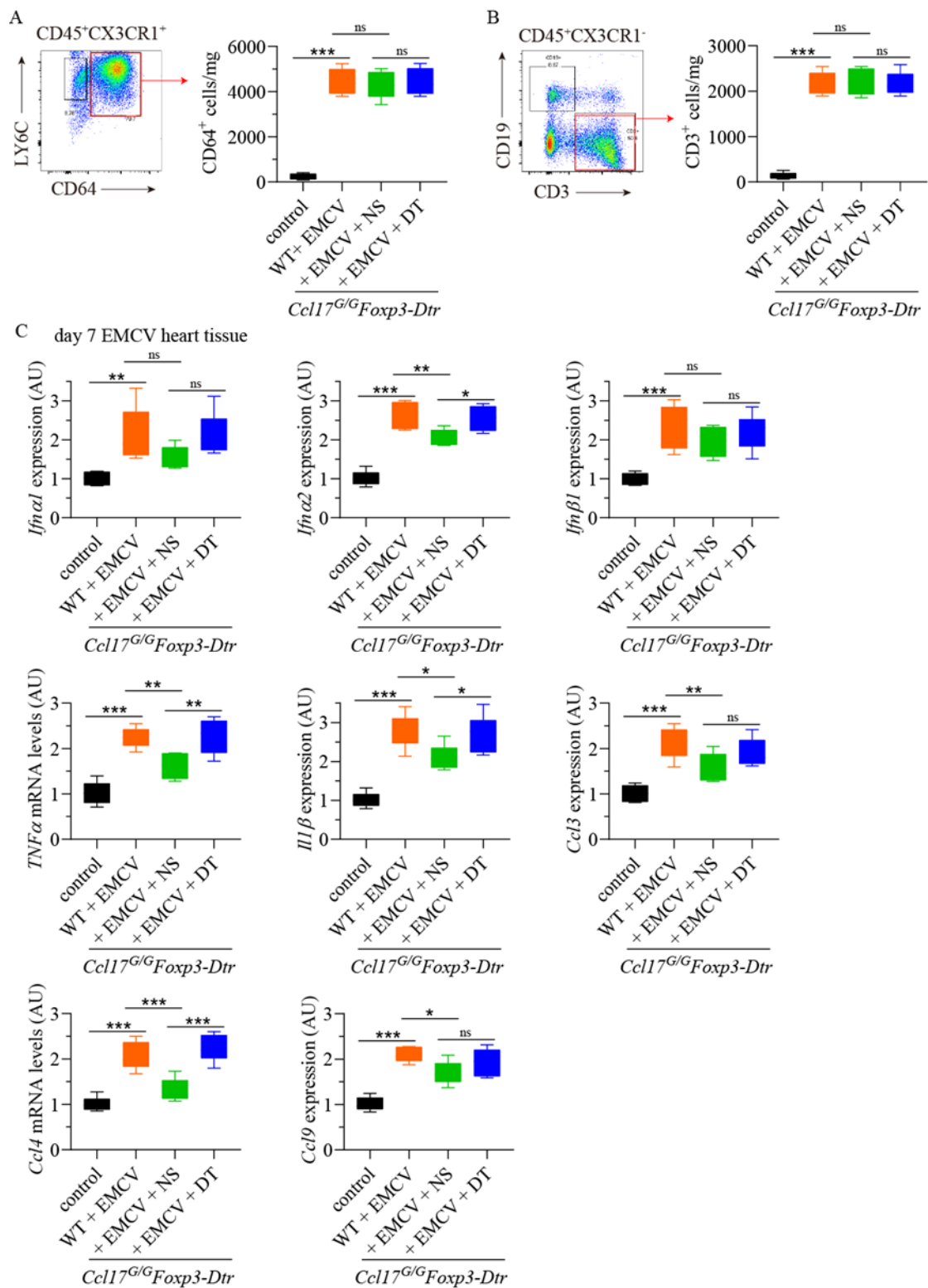


Effect of Treg depletion on survival rate and heart remodeling. **A.** Cardiac Treg deletion strategy and efficiency confirmation by flow cytometry. **B.** Survival rate comparisons

between encephalomyocarditis viruses (EMCV) treated wild type group (WT + EMCV, N=26) and EMCV together with diphtheria toxin (DT) treated *Ccl17<sup>green fluorescent protein</sup>/green fluorescent protein* crossed forkhead box P3-diphtheria toxin receptor (*Ccl17<sup>G/G</sup>Foxp3-Dtr*) mice (*Ccl17<sup>G/G</sup>Foxp3-Dtr* + EMCV + DT group, N=27). **C.** Representative staining images for cardiomyocytes (green), DNA-damaged cells (red) and DAPI (4',6-diamidino-2-phenylindole; blue) showing cardiomyocytes death in non-infected control hearts, DT (n=12) and NS (n=12) treated *Ccl17<sup>G/G</sup>Foxp3-Dtr* mice 14 days after EMCV injection. **D.** Effect of Treg deletion on expressions of fibrosis markers *collagen 1a1* & *3a1* in hearts. **E.** Representative trichrome staining images of non-infected control heart. **F.** Effect of Treg deletion on expressions of hypertrophy markers Natriuretic Peptide A&B (NPPA&B), and myosin heavy chain 7 (MYH7) in hearts. **G.** Representative wheat germ agglutinin (WGA) stained images showing cardiomyocytes in cross-section (red, left panel) and quantification of cardiomyocyte cross-sectional area (right panel) in hearts of non-infected control mice and *Ccl17<sup>G/G</sup>Foxp3-Dtr* mice 28 days after EMCV, DT or NS treatments. For **A**, **C**, **D**, *Ccl17<sup>G/G</sup>* mice were crossed with *Foxp3-Dtr* mice to generate *Ccl17<sup>G/G</sup>Foxp3-Dtr* mice in which Tregs could be deleted after DT administration. Wild type (*Ccl17<sup>+/+</sup>*) mice were treated with normal saline (NS) as control. *Ccl17<sup>G/G</sup>Foxp3-Dtr* mice were treated with EMCV+NS or EMCV + DT as experimental groups. All data are mean ± SD. For multiple comparisons didn't present normality (**A**), nonparametric Kruskal-Wallis test was performed. For other multiple comparisons presented normality and showed equal variance (**C**), ordinary one-way ANOVA following Tukey's multiple comparisons tests were performed. For survival rate comparison in A, Log rank (Mantel-Cox test) was performed. For all data, "ns" indicate non-significance, \* indicate  $P < 0.05$ , \*\* indicate  $P < 0.01$ , and \*\*\* indicate  $P < 0.001$ .



**Figure S7.** Effect of *Ccl17* deletion and Treg depletion on macrophage and T cell abundance and inflammatory gene expression.



Effect of Treg depletion on macrophages & T cells abundance and gene expression in heart. **A.** Flow cytometry demonstrating the number of cluster of differentiation 64 (CD64)<sup>+</sup> macrophages per mg heart tissue 7 days after encephalomyocarditis viruses

(EMCV) infection. **B.** Flow cytometry demonstrating the number of CD3<sup>+</sup> T cells per mg heart tissue 7 days after EMCV infection. **C.** qRT-PCR showing the expression of interferon  $\alpha 1$  (*Ifna1*), *Ifna2*, *Ifnb1*, tumor necrosis factor (*Tnfa*), interleukin  $1\beta$  (*Il1b*), macrophage inflammatory protein 1-a (*Ccl3*), macrophage inflammatory protein *1b* (*Ccl4*) and macrophage inflammatory protein  $1\gamma$  (*Ccl9*). For **A**, **B** and **C**, *Ccl17<sup>green</sup> fluorescent protein / green fluorescent protein* mice were crossed with forkhead box P3-diphtheria toxin receptor to generate *Ccl17<sup>G/G</sup> Foxp3-Dtr* mice in which Tregs could be deleted after DT administration. Wild type (*Ccl17<sup>+/+</sup>*) mice treated with normal saline (as control) or EMCV were compared with *Ccl17<sup>G/G</sup> Foxp3-Dtr* mice treated with EMCV + NS or EMCV + DT. Hearts were harvested on day 7 for analysis. N=6 per experimental group and all data are mean  $\pm$  SD. For multiple comparisons didn't present normality (**A**), nonparametric Kruskal-Wallis test was performed. For other multiple comparisons presented normality and showed equal variance (**B**, **C**), ordinary one-way ANOVA following Tukey's multiple comparisons tests were performed. For all data, "ns" indicate non-significance, \* indicate  $P < 0.05$ , \*\* indicate  $P < 0.01$ , and \*\*\* indicate  $P < 0.001$ .